Mon. Not. R. Astron. Soc. **000**, 1–29 (2016) Printed 13 October 2016 (MN LATEX style file v2.2)

The clustering of galaxies in the completed SDSS-III Baryon Oscillation Spectroscopic Survey: theoretical systematics and Baryon Acoustic Oscillations in the galaxy correlation function

arXiv:1610.03506v1 [astro-ph.CO] 11 Oct 2016

Mariana Vargas-Magaña[1,2,3], Shirley Ho[2,3,4,5], Antonio J. Cuesta[6], Ross O'Connell[2,3], Ashley J. Ross[7], Daniel J. Eisenstein[8], Will J. Percival[9], Jan Niklas Grieb[10,11], Ariel G. Sánchez[10], Jeremy L. Tinker[12], Rita Tojeiro[13], Florian Beutler[9], Chia-Hsun Chuang[14,15], Francisco-Shu Kitaura[14,15,5], Francisco Prada[14,16,17], Sergio A. Rodríguez-Torres[14,16,17], Graziano Rossi[18], Hee-Jong Seo[19], Joel R. Brownstein[20], Matthew Olmstead[21], Daniel Thomas[9]

[1] *Instituto de Física, Universidad Nacional Autónoma de México, Apdo. Postal 20-364, México.*
[2] *Departments of Physics, Carnegie Mellon University, 5000 Forbes Ave., Pittsburgh, PA 15217*
[3] *McWilliams Center for Cosmology, Carnegie Mellon University, 5000 Forbes Ave., Pittsburgh, PA 15217*
[4] *Lawrence Berkeley National Lab, 1 Cyclotron Rd, Berkeley CA 94720, USA*
[5] *Departments of Physics and Astronomy, University of California, Berkeley, CA 94720, USA*
[6] *Institut de Ciències del Cosmos (ICCUB), Universitat de Barcelona (IEEC-UB), Martí i Franquès 1, E08028 Barcelona, Spain*
[7] *Center for Cosmology and AstroParticle Physics, The Ohio State University, Columbus, OH 43210, USA*
[8] *Harvard-Smithsonian Center for Astrophysics, 60 Garden St., Cambridge, MA 02138, USA*
[9] *Institute of Cosmology & Gravitation, Dennis Sciama Building, University of Portsmouth, Portsmouth, PO1 3FX, UK*
[10] *Universitäts-Sternwarte München,Ludwig-Maximilians-Universität München, Scheinerstraße 1, 81679, München, Germany*
[11] *Max-Planck-Institut für extraterrestrische Physik, Postfach,1312, Giessenbachstr., 85741 Garching, Germany*
[12] *Center for Cosmology and Particle Physics, New York University, New York, NY 10003, USA*
[13] *School of Physics and Astronomy, University of St Andrews, St Andrews, KY16 9SS, UK*
[14] *Instituto de Física Teórica, (UAM/CSIC), Universidad Autónoma de Madrid, Cantoblanco, E-28049 Madrid, Spain*
[15] *Leibniz Institut für Astrophysik Potsdam (AIP), An der Sternwarte 16, D-14482 Potsdam, Germany*
[16] *Campus of International Excellence UAM+CSIC, Cantoblanco, E-28049 Madrid, Spain*
[17] *Departamento de Física Teórica M8, Universidad Autonóma de Madrid (UAM), Cantoblanco, E-28049, Madrid, Spain*
[18] *Department of Physics and Astronomy, Sejong University, Seoul, 143-747, Korea.*
[19] *Department of Physics and Astronomy, Ohio University, 251B Clippinger Labs, Athens, OH 45701, USA*
[20] *Department of Physics and Astronomy, University of Utah, 115 S 1400 E, Salt Lake City, UT 84112, USA*
[21] *Department of Chemistry and Physics, King's College, 133 North River St, Wilkes Barre, PA 18711, USA*

13 October 2016

ABSTRACT

We investigate the potential sources of theoretical systematics in the anisotropic Baryon Acoustic Oscillation (BAO) distance scale measurements from the clustering of galaxies in configuration space using the final Data Release (DR12) of the Baryon Oscillation Spectroscopic Survey (BOSS). We perform a detailed study of the impact on BAO measurements from choices in the methodology such as fiducial cosmology, clustering estimators, random catalogues, fitting templates, and covariance matrices. The theoretical systematic uncertainties in BAO parameters are found to be 0.002 in in the isotropic dilation α and 0.003 in in the quadrupolar dilation ϵ. We also present BAO-only distance scale constraints from the anisotropic analysis of the correlation function. Our constraints on the angular diameter distance $D_A(z)$ and the Hubble parameter $H(z)$ including both statistical and theoretical systematic uncertainties are 1.5% and 2.8% at $z_{\rm eff} = 0.38$, 1.4% and 2.4% at $z_{\rm eff} = 0.51$, and 1.7% and 2.6% at $z_{\rm eff} = 0.61$. This paper is part of a set that analyses the final galaxy clustering dataset from BOSS. The measurements and likelihoods presented here are cross-checked with others BAO analysis in Alam et al. (2016). The systematic error budget concerning the methodology on post-reconstruction BAO analysis presented here is used in Alam et al. (2016) to produce the final cosmological constraints from BOSS.

Key words: reconstruction; galaxies; galaxies: statistics; cosmological parameters; large-scale structure of Universe

1 INTRODUCTION

The Baryon Oscillation Spectroscopic Survey (BOSS, (Dawson et al. 2012)) Data Release 12 (DR12, Alam et al. 2015) is the largest galaxy spectroscopic survey available to date providing the most precise measurements on Baryonic Acoustic Oscillations (BAO). Since the previous Data Release, (i.e. DR11), the scientific goal of the experiment of 1 per cent measurement in the distance measurements was achieved. eBOSS Dawson et al. (2016) is going to expand the redshift range of the distance measurements with precision similar to its predecessor BOSS. Improvements on this precision are expected for the next generation of dark energy experiments, (Stage IV from the Dark Energy Task Force). Planned large galaxy surveys such as the Dark Energy Spectroscopic Instrument (DESI) (Mostek et al. 2012; Levi et al. 2013), Euclid (Laureijs 2009; Laureijs et al. 2011), LSST (LSST Dark Energy Science Collaboration 2012), SKA (Bull et al. 2015), and WFIRST (Spergel et al. 2013a,b) are expected to measure $H(z_{\rm eff})$ and $D_A(z_{\rm eff})$ to subpercent level. In order to approach this level of precision, a careful investigation of potential sources of systematic effects is required.

In this work, we aim to examine the methodology of Baryon Acoustic Oscillation (BAO) analysis, focusing on the various potential sources of theoretical systematics. We explore these systematic uncertainties by performing a BAO anisotropic analysis in configuration space over a large number of realistic mock catalogues generated for the final analysis of the BOSS galaxy clustering. The studies performed in this work provide a basis for the systematic error included in the final BAO measurements of BOSS DR12 galaxy samples (Alam et al. 2016). The observational systematics in BOSS combined galaxy catalogues are covered in Ross et al. (2016). This work is part of the final analysis of BOSS DR12 completed samples for the BAO and Redshift-Space Distortions (RSD) analyses (Ross et al. 2016; Sánchez et al. 2016a; Beutler et al. 2016a,b; Grieb et al. 2016; Satpathy et al. 2016, companion papers).

In order to clarify the applicability of this analysis we remark to the reader that this work is focused on configuration space analysis and heavily focused on post-reconstruction results, whereas Alam et al. (2016) uses the average of Fourier space and configuration analysis, and also includes pre-reconstruction data for the full shape analysis. Thus, the systematics budget account derived from this study is relevant only for the BAO-only fits, and in particular in configuration space and post-reconstruction. We also provide results pre-reconstruction, however the most part of the analysis will be centred in the post-reconstruction results.

The outline of the paper is as follows. In Section 2 we describe the data and mock catalogues used for the studies and include a brief description of the anisotropic BAO methodology. In Section 3 we define the fiducial (base) methodology and we present the procedure we follow to analyze the variations of the methodology in order to account a error budget. In Sections 4-9 we revisit the potential sources of systematics following step-by-step the anisotropic BAO analysis methodology. Thus, Section 4 is devoted to testing different 2-point estimators in configuration space (multipoles, wedges, and ω-estimators); Section 5 studies the effect of the random catalogues used on the 2-point estimator for the multipoles case; Section 6 explores the effects of the covariance matrix; Section 7 revisit the effect of smoothing scale in the reconstruction of the linear density field and its impact on BAO anisotropic analysis; Section 8 tests the effect of the assumed fiducial cosmology in the analysis; Section 9 studies the systematics related to the anisotropic fitting methodology and modelling. In Section 10 we apply the variations of the methodology to the BOSS DR12 measurements. In Section 11 we discuss the methodology to establish a systematic error budget for the DR12 measurements. Finally, in Section 12 we present the final constraints on the angular diameter distance $D_A(z)$ and the Hubble parameter distance $H(z)$ including the theoretical systematic uncertainties; we conclude in Section 13.

2 METHODOLOGY

2.1 Galaxy Sample Creation: BOSS Final Dataset

The SDSS-III (Eisenstein et al. 2011) BOSS (Dawson et al. 2012) survey uses the Sloan Foundation 2.5-meter telescope at Apache Point Observatory (Gunn et al. 1998, 2006). The targets use wide-field CCD photometry in five passbands u,g,r,i,z (Fukugita et al. 1996). The spectra are obtained using the double-armed BOSS spectrograph (Smee et al. 2013). The data is then reduced using the algorithms described in Bolton et al. (2012). We use BOSS DR12 (Alam et al. 2015) galaxy sample and provide a brief description. For detailed information, please refer to Alam et al. (2016) and Reid et al. (2016). The BOSS galaxy samples have traditionally included the Constant Stellar Mass sample, or CMASS, covering redshifts in the range $0.43 < z < 0.70$ and a fiducial redshift of 0.57, and the low-redshift sample, or LOWZ, covering redshifts of $0.15 < z < 0.43$ with an effective redshift of 0.32 (Reid et al. 2016). Also included in the final analysis are the early LOWZ samples that were targeted with a different target selection algorithm; this set is called 'LOWZ Early'. For the final analysis we combine all these samples (hereafter 'BOSS Combined Sample') and define three redshift slices that overlap by $\sim 200\ h^{-1}$Mpc and are chosen to be approximately equal in effective volume. These are: $V_{\rm low}$, which includes galaxies in the redshift range $z = 0.2 - 0.5$ (denoted hereafter 'Bin 1'); $V_{\rm mid}$, which considers the redshift range $z = 0.4 - 0.6$ (denoted hereafter 'Bin 2'); and $V_{\rm high}$, which includes the redshift range $z = 0.5 - 0.75$ (denoted hereafter 'Bin 3'). $V_{\rm mid}$ completely overlaps with the other two, but also contains the peak of number density. The effective redshifts $z_{\rm eff}$ for each bin are 0.38, 0.51, and 0.61, respectively. The three different redshift bins have 604001, 686370, and 594003 galaxies, respectively.

2.2 Mitigating Observational Systematics in the Galaxy Catalogues

Extensive discussions of observational systematics in BOSS galaxy catalogues are available in Ross et al. (2011, 2012), and in the final BOSS data release. (Ross et al. 2016) describes the detailed observational systematics in BOSS combined galaxy catalogues. We will use all of the observational systematics weights that are determined in Ross et al. (2016) throughout our entire work.

2.3 Mock Catalogue Generation

In this paper, we use SDSS III-BOSS mock catalogues extensively. They consist of PTHALOS (Manera et al. 2013a), QPM (White, Tinker & McBride 2014) and MD-PATCHY (Kitaura et al. 2015).

2.3.1 PTHALOS Mocks

PTHALOS mocks (Manera et al. 2013a) are based on Second Order Lagrangian perturbation Theory (2LPT) for the density fields. The method for generating galaxy mocks follows PTHALOS methodology described in Scoccimarro & Sheth (2002). The mocks were

generated at a fixed redshift $z = 0.55$ and in cubic boxes (L = 2400 h^{-1}Mpc) using 1280^3 dark matter particles. The halos were found using a friends-of-friends algorithm and their masses were calibrated using N-body simulations. To populate the halos with galaxies, a Halo Occupation Distribution prescription was used, previously calibrated to match the observed clustering at small scales (30–80 h^{-1}Mpc). The angular and radial masks from DR10/DR11 were applied to match the survey footprint on the original boxes. The mocks include redshift distortions but do not include other systematic corrections such as close-pair collisions, stellar density correlations, or redshift evolution. A full description of the mocks can be found in Manera et al. (2013a). The cosmology is $\Omega_M = 0.274, \Omega_\Lambda = 0.726, \Omega_b = 0.045, \sigma_8 = 0.8$ and $h = 0.7$.

2.3.2 QPM Mocks

Quick Particle Mesh (QPM) mocks were generated for BOSS clustering analysis. These mock catalogues use low mass and force resolution particle-mesh simulations employing 1280^3 particles in a (2560 h^{-1}Mpc)^3 box ran with large time steps. At selected times, the particles and their local density smoothed on 2 h^{-1}Mpc scales were dumped; these particles were then sampled (with a density-dependent probability) to form a set of mock halos that are then populated using a halo occupation distribution (White, Tinker & McBride 2014). The mock catalogues match the observed number density of BOSS galaxies and follow the radial and angular selection functions of BOSS galaxy samples. The cosmology is $\Omega_M = 0.29$, $\Omega_\Lambda = 0.71$, $\Omega_b = 0.048$, $\sigma_8 = 0.8$ and $h = 0.7$.

We use two different versions of the QPM mocks: 1) a version that matches the DR12 CMASS samples used in previous analyses (Cuesta et al. 2016; Vargas-Magana et al. 2015; Gil-Marín et al. 2016) and 2) a new set of mocks for the DR12 combined sample that match the samples used for the final BOSS clustering analysis. The mocks combine in an optimal way all BOSS galaxy data, including, CMASS, LOWZ, and early chunks not used in previous BOSS analyses referred to as "LOWZ Early" data. These samples are used in the final BAO/RSD analyses (Ross et al. 2016; Sánchez et al. 2016a; Beutler et al. 2016a,b; Grieb et al. 2016; Satpathy et al. 2016, companion papers).

2.3.3 MULTIDARK-PATCHY Mocks

MD-PATCHY mocks are based on Augmented Lagrangian Perturbation Theory and a non-linear bias stochastic scheme (Kitaura, Yepes & Prada 2014), where the bias parameters are fitted to match the proper clustering of the BigMultiDark Planck simulation for each redshift snapshot (Klypin, Yepes, Gottlober, Prada, &Hess 2016). The HADRON code was used for mass assignment to halos (Zhao, Kitaura, Chuang, Prada, Yepes, & Tao 2015). Light-cone mocks are built using the SUGAR code (Rodriguez-Torres et al. in preparation) and the Mock-Factory products (https://github.com/mockFactory). These mocks were designed to reproduce the observed evolution of clustering, and its dependence with stellar mass. Initial conditions for the MD-PATCHY code were created using BigMultiDark simulation (also described in Klypin, Yepes, Gottlober, Prada, &Hess 2016). The cosmology is based on Planck (Planck Collaboration et al. 2015b): Ω_M= 0.307115, Ω_Λ= 0.692885, $\Omega_b = 0.048$, σ_8 = 0.8288 and $h = 0.6777$. We used Version 6C of the mocks (where "C" stands for "Covariance matrix" of the clustering measurements). These mocks are tuned to reproduce the clustering of observed data in terms of 1-point, 2-point, and 3-point clustering statistics in redshift space.

2.4 Fiducial Cosmology

For the analysis of our DR12 combined sample defined in Section 2.1, we assume the following fiducial cosmology: $\Omega_m = 0.31$, $\Omega_\Lambda = 0.69$, $\Omega_k = 0$, $\Omega_b h^2 = 0.022$, $\Omega_\nu h^2 = 0.00064$, $w = -1$, $w_a = 0$, $h = 0.676$, $n_s = 0.97$, and $\sigma_8 = 0.8$. Section 8 tests the effect of using different fiducial cosmologies in the analysis. The cosmologies explored in this case are presented in Table 11.

2.5 Choosing Estimators

Anisotropic BAO analysis requires the computation of the 2D correlation function $\xi(r, \mu)$ (or power spectrum $P(k, \mu)$). Using the full 2D correlation function is impractical since it requires a covariance matrix that is precise for a relatively large number of parameters. There are, however, several ways of compressing the information that are usually implemented in the different BAO analyses. In configuration space, these include the multipole method (Xu et al. 2012a,b), the ω_l statistic (Xu et al. 2010), and the wedges method (Kazin et al. 2013; Sánchez et al. 2013a). We will define a few parameters to make our discussion of estimators more transparent. We first compute the two-point correlation function in 2D, decomposing the separation r between two galaxies into two components: parallel to line of sight $r_{||}$ and perpendicular to line of sight, $r_\perp$, where r is defined as follows:

$$r^2 = r_{||}^2 + r_\perp^2. \tag{1}$$

We denote θ the angle between the galaxy pair separation and the LOS direction, and we define $\mu = \cos\theta$ so that:

$$\mu^2 = \cos^2\theta = \frac{r_{||}^2}{r^2}. \tag{2}$$

The 2D-correlation function $\xi(r, \mu)$ (for the pre-reconstructed case) is then computed using Landy-Szalay estimator (Landy & Szalay 1993) that reads as follows:

$$\xi(r, \mu) = \frac{DD(r, \mu) - 2DR(r, \mu) + RR(r, \mu)}{RR(r, \mu)}, \tag{3}$$

where $DD(r, \mu)$, $RR(r, \mu)$, and $DR(r, \mu)$ are the number of pairs of galaxies which are separated by a radial separation r and angular separation μ from data-data, random-random, and data-random pairs, respectively.

After computing the two-point correlation function in 2D, we can then compress it into multipoles, wedges, and ω_l.

2.5.1 Multipoles

The multipoles are Legendre moments of the 2D correlation function $\xi(r, \mu)$. They can be computed through the following equation:

$$\xi_\ell(r) = \frac{2\ell + 1}{2} \int_{-1}^{+1} d\mu\, \xi(r, \mu)\, L_\ell(\mu), \tag{4}$$

where $L_\ell(\mu)$ is the ℓ-th order Legendre polynomial. We focus primarily on the monopole and the quadrupole ($\ell = 0$ and $\ell = 2$), although we will have a discussion on hexadecapole ($\ell = 4$) in this work.

2.5.2 Clustering Wedges

The clustering wedges are an integral of the correlation function over a range of μ:

$$\xi_{\Delta\mu}(r) = \frac{1}{\Delta\mu} \int_{\mu_{min}}^{\mu_{min}+\Delta\mu} d\mu\, \xi(r, \mu). \tag{5}$$

Table 1. Fiducial cosmologies used in this work.

Cosmology	Ω_{CDM}	Ω_M	Ω_B	Ω_Λ	h	Samples
PTHALOS	0.228286	0.274	0.0457143	0.726	0.7	CMASS DR11
QPM	0.244143	0.29	0.0458571	0.71	0.7	CMASS DR11/DR12
Alam et al. (2016)	0.261857	0.31	0.0481426	0.69	0.676	COMBINED DR12
MD-PATCHY	0.258909	0.307115	0.048206	0.692885	0.676	-

We choose $\Delta\mu = 0.5$ in our work, following Kazin et al. (2012, 2013) and Sánchez et al. (2013a). We define, in particular, the wedge parallel to line of sight to be $\xi_{||}(r)$ for $0.5 < \mu < 1$ and the wedge perpendicular to line of sight to be $\xi_\perp(r)$ for $0 < \mu < 0.5$.

The clustering wedges and multipoles are complementary bases as shown in Kazin et al. (2012); they can be related (discarding multipoles with $\ell > 4$) by:

$$\xi_\perp(r) = \xi_0(r) - \frac{3}{8}\xi_2(r) + \frac{15}{128}\xi_4(r), \tag{6}$$

$$\xi_\parallel(r) = \xi_0(r) + \frac{3}{8}\xi_2(r) - \frac{15}{128}\xi_4(r), \tag{7}$$

2.5.3 *ω-Estimator*

As in Xu et al. (2010), we define ω_l as the redshift space correlation function, $\xi_s(r,\mu)$, convolved with a compact and compensated filter $W_\ell(r,\mu,r_c)$ as a function of characteristic scale r_c:

$$\omega_l = i^\ell \int d^3r\, \xi_s(r,\mu)\, W_\ell(r,\mu,r_c), \tag{8}$$

where we have taken advantage of the orthogonality of the Legendre polynomials and set $W_\ell(r,\mu,r_c) = W_\ell(r,r_c)\, L_\ell(\mu)$. Following Padmanabhan et al. (2007) and Xu et al. (2010), we define a smooth, low order, compensated filter independent of ℓ:

$$W_\ell(x) = (2x)^2 (1-x)^2 \left(\frac{1}{2} - x\right) \frac{1}{r_c^3}, \tag{9}$$

where $x = (r/r_c)^3$. This choice of filter gives the ω_l statistic several advantages. By design, ω_l probes a narrow range of scales near the BAO feature and is not sensitive to large scale fluctuations or to poorly measured or modelled large scale modes (Xu et al. 2010).

2.6 Anisotropic Parametrization: α and ϵ

To analyze the anisotropic BAO signal, we need a model with a parametrization of the anisotropic clustering signal. There are two sources of anisotropies: the RSD and the anisotropies generated from assuming a wrong cosmology, also known as the Alcock-Paczynski effect (AP) (Alcock & Paczynski 1979). As $D_A(z)$ and H(z) depend on the cosmological parameters differently, if one assumes a fiducial cosmology different from the one that matches the sample, $H(z)$ and $D_A(z)$ will generate artificial anisotropies in the clustering along Line-of-Sight (LOS) and perpendicular directions (Matsubara et al. 2000; Okumara et al. 2008; Padmanabhan & White 2009; Seo et al. 2008; Xu et al. 2012b).

For the extraction of the cosmological information, we follow the methodology described in Xu et al. (2012b) and Anderson et al. (2013), which derives measurements of the isotropic dilation of the coordinates parametrized by α and the anisotropic warping of the coordinates parametrized by ϵ. Here α and ϵ parametrize the geometrical distortion derived from assuming a wrong cosmology when calculating the galaxy correlation function. The parameters α and ϵ are defined as Padmanabhan & White (2009):

$$\begin{aligned} \alpha &= \alpha_\perp^{2/3} \alpha_{||}^{1/3}, \\ 1+\epsilon &= \left(\frac{\alpha_{||}}{\alpha_\perp}\right)^{1/3}. \end{aligned} \tag{10}$$

where $\alpha_\perp$ and $\alpha_{||}$ are defined in terms of dilation in the transverse and line-of-sight directions, given by a difference between the fiducial cosmology and the "true cosmology"[1].

The parameters α and ϵ are related to $D_A(z)/r_s$ and $cz/(H(z)r_s)$ where $D_A(z)$ is the angular diameter distance to redshift z, r_s is the sound horizon at radiation drag, and $H(z)$ is the Hubble parameter. Finally, $\alpha_\perp$ and $\alpha_{||}$ are related to $D_A(z)/r_s$ and $cz/(H(z)r_s)$ in the following way:

$$\alpha_\perp = \frac{D_A(z) r_s^{\rm fid}}{D_A^{\rm fid} r_s}, \tag{11}$$

and

$$\alpha_{||} = \frac{H^{\rm fid}(z) r_s^{\rm fid}}{H(z) r_s}. \tag{12}$$

2.7 BAO Fitting, From Correlation Functions to Distance Estimates

2.7.1 *Nonlinear Model for the Correlation Function*

For modelling the non linear correlation function we follow Xu et al. (2012a,b). We start from a template for the 2D nonlinear power spectrum (Fisher et al. 1994) considered as follows:

$$P(k,\mu) = (1+\beta\mu^2)^2 F(k,\mu,\Sigma_s) P_{\rm NL}(k,\mu). \tag{13}$$

The term $(1+\beta\mu^2)^2$ corresponds to the Kaiser model for large scale redshift space distortions. $F(k,\mu,\Sigma_s)$ is the streaming model for Fingers-of-God (FoG) given by:

$$F(k,\mu,\Sigma_s) = \frac{1}{(1+k^2\mu^2\Sigma_s^2)} \tag{14}$$

where Σ_s is the streaming scale. $P_{\rm NL}(k)$ is the non linear power spectrum. In this work, we consider the de-wiggled power spectrum $P_{\rm dw}$, defined as:

$$\begin{aligned} P_{\rm dw}(k,\mu) = \; & [P_{\rm lin}(k) - P_{\rm nw}(k)] \\ & \times \exp\left[-\frac{k^2\mu^2\Sigma_{||}^2 + k^2(1-\mu^2)\Sigma_\perp^2}{2}\right] + P_{\rm nw} \end{aligned} \tag{15}$$

[1] Note that $\alpha = 1$ and $\epsilon = 0$ for the mocks, if we use their natural cosmology as the fiducial cosmology for the analysis.

where $P_{\rm lin}(k)$ is the linear theory power spectrum and $P_{\rm nw}(k)$ is a power spectrum without the acoustic oscillations (Eisenstein & Hu 1998). $\Sigma_{||}$ and $\Sigma_{\perp}$ are the radial and transverse components of the standard Gaussian damping of BAO Σ_{NL}.

In order to get the templates for the multipoles, we then decompose the 2D power spectrum into its Legendre moments:

$$P_{l,t}(k) = \frac{2l+1}{2}\int_{-1}^{1} P_t(k,\mu)L_l(\mu)d\mu, \tag{16}$$

which can then be transformed to configuration space using

$$\xi_{l,t}(r) = i^l \int \frac{k^3 d\log(k)}{2\pi^2} P_{l,t} j_l(kr), \tag{17}$$

where $j_l(kr)$ is the l-th order spherical Bessel function and $L_l(\mu)$ is the l-th order Legendre polynomial.

The model we fit to our observed multipoles $\xi_0(r)$ and $\xi_2(r)$ are:

$$\begin{aligned}\xi_0(r) &= B_0^2\xi_{0,\rm t}(r) + A_0(r),\\ \xi_2(r) &= \xi_{2,\rm t}(r) + A_2(r),\end{aligned} \tag{18}$$

where

$$A_\ell(r) = \frac{a_{\ell,1}}{r^2} + \frac{a_{\ell,2}}{r} + a_{\ell,3};\ \ell = 0, 2, \perp, \| \tag{19}$$

These $A_\ell(r)$ terms are used to marginalise out broadband (shape) information through the $a_{\ell,1}\ldots a_{\ell,3}$ nuisance parameters.

Our model for wedges is derived from the templates for ξ_ℓ by applying Eq. 6 (derived in Kazin et al. (2012)), discarding contributions from multipoles with $\ell > 4$ to the expected observations for ξ_ℓ given in Eq. 18.

Our models for ω_ℓ are derived from the templates for ξ_ℓ by applying Eq. 8 with the filter defined in Eq. 9 to the expected observations for ξ_ℓ given in Eq. 18. In short, ω_ℓ is a filtered integral of ξ.

As in the multipoles fitting, when fitting ω_ℓ, we fit $\omega_0\,(r_c)$ and $\omega_2\,(r_c)$ simultaneously with the same nonlinear parameters.

In order to find the best-fit values of α and ϵ, we minimise the χ^2 function,

$$\chi^2 = (\vec{m} - \vec{d})^T C^{-1} (\vec{m} - \vec{d}), \tag{20}$$

where $\vec{m}$ is the model and $\vec{d}$ is the data correlation function (binned in radial bins). We scale the inverse sample covariance matrix estimated from the mocks, C_s^{-1}, using the equation:

$$C^{-1} = C_s^{-1}\frac{N_{\rm mocks} - N_{\rm bins} - 2}{N_{\rm mocks} - 1}, \tag{21}$$

correcting for the fact that it is a biased estimate of the true inverse covariance matrix C^{-1} Hartlap et al. (2007); Percival et al. (2014) Error estimates for α and ϵ are obtained by evaluating χ^2 on a grid in these two parameters to map out the likelihood surface. Assuming the likelihood surface is Gaussian allows us to estimate σ_α and σ_ϵ as the standard deviations of the marginalised likelihoods of α and ϵ, respectively.

2.8 Reconstruction

Reconstruction has become part of the essential toolkit for BAO analysis (Eisenstein et al. 2007b,a; Padmanabhan et al. 2012; Vargas-Magana et al. 2014; Burden et al. 2014, 2015; Vargas-Magana et al. 2015). The reconstruction algorithm has proved to be effective in partially correcting the effects of nonlinear evolution increasing the statistical precision of the measurements. The main idea of reconstruction is to use information encoded in the density field to estimate the displacement field and use this displacement field to move back the particles and partially remove the effect of the nonlinear growth of structure. This is possible since nonlinear evolution of the density field at the BAO scale is dominated by the infall velocities; these bulk flows are generated by the same structures observed in the density field. The algorithm used here is similar in spirit to Padmanabhan et al. (2012); our particular implementation is the same as in Vargas-Magana et al. (2015), where a detailed description can be found.

Table 2. Fiducial Methodology

Analysis	Fiducial Methodology
Estimator	Multipoles up to $\ell = 2$
Randoms	Post-reconstruction: $7x$ SS, $50x$ SR (covariance mocks)
Randoms	Post-reconstruction: $50x$ (data)
Covariance	Sample Covariance from 1000 MD-Patchy mocks
Fid. Cosmo.	$\Omega_m = 0.31$, $\Omega_\Lambda = 0.69$, $\Omega_b h^2 = 0.022$
Alam et al. (2016).	$h = 0.676$, $n_s = 0.97$, and $\sigma_8 = 0.8$
Reconstruction	Smoothing scale, $15h^{-1}$Mpc
Modelling	Gaussian Damping Model
Modelling	Fitting Range: [55, 160] h^{-1}Mpc
Modelling	Binning: 5 h^{-1}Mpc
Modelling	De-Wiggled P(k) template
Modelling	α-ϵ parametrization
Modelling	Nuisance terms: 3-term $A_l(r)$

3 THEORETICAL SYSTEMATICS OF THE BAO ANALYSIS

In Sections 4-9, we will go through the following steps of the BAO analysis and discuss the potential systematics associated with each step.

(i) 2-point statistics Estimators
(ii) Random Set
(iii) Covariance
(iv) Reconstruction
(v) Fiducial Cosmology
(vi) Modelling of the 2-point statistics

Our goal is to establish a theoretical systematic error budget by considering the effect on the BAO measurements against variations on the methodology. In order to give a reference frame to the reader, we start defining our Fiducial methodology in Table 2. We describe in detail the results of our fiducial methodology in Section 4. The results of the fiducial methodology are characterized by the mean $\bar{x}$ and standard deviation S_x of the distributions of the best parameters (α, ϵ) and their uncertainties (σ_α and σ_ϵ). For the variants of the methodology we will present only the variations of the distributions compared with the fiducial methodology.

In Sections 4-9, for convenience of the reader, we follow the same structure: we start reminding the reader what is the fiducial choice; we then present which variations of the methodology we explore in the section, and we finish presenting the results. For exploring the systematic errors associated to each step, we perform the anisotropic fits to the mocks catalogues following the fiducial methodology and also we perform the fits for each variant of the methodology. When analyzing the results, we determine which

variations produce statistically significant biases on the measurement, the bias is defined as $b_x = \bar{x} - x_{\rm exp}$, where $\bar{x}$ is the mean of the variable x and the variable $x = \alpha, \epsilon, \sigma_\alpha, \sigma_\epsilon$; $x_{\rm exp}$ is the value expected for the variable. To determine the systematic error associated to one step of the analysis we compared each variation to the methodology with the fiducial case and we determine the variations:

$$\Delta_x = \bar{x}_{\rm var} - \bar{x}_{\rm fid}. \quad (22)$$

The systematic errors associated to each step will be used in Section 11 to establish the final systematic error budget. For the final error budget we will account only the choices that do not generate significant shifts (bias) in the best fits parameters. We expect all of them will make a small contribution to the final error budget for BOSS samples; however an accurate account of the potential sources of systematics is necessary in the current era of per-cent precision in the distances measurements.

As an additional result in cases where the uncertainties are affected by the variation in the methodology we also quote the differences in the error distributions using the same notation definition 22.

4 ESTIMATORS

In this section, we quantify the systematic error related to the estimator choice. We followed two approaches: in the first part of the section, we explored how using different estimators in configuration space generate variations in the anisotropic fits. In the second part, we compare with the analysis performed with combined sample DR12. We compare first with a analog analysis performed in Configuration Space using multipoles (Ross et al. 2016), we also include results from analysis using multipoles in Fourier Space (Beutler et al. (2016a)) and also to compare with the consensus results presented in Alam et al. (2016).

For the first part, we implement in the same pipeline the different estimators so that the variations will be dependent only on the estimator and not on other details of the fits that could vary between different clustering analyses. The estimators used in our fiducial methodology are the multipoles. In addition to the multipoles analysis, we analyzed the wedges ($\xi_{\parallel,\perp}$) and ω_ℓ estimators (all of them explained in the methodology section).

The multipoles measurements are shown in Figure 1; the top panels show the mean monopole, the intermediate panels display the mean quadrupole, and the bottom panels show the mean hexadecapole from 1000 MD-PATCHY Combined mocks pre (left) and post reconstruction (right) for the three redshift bins. The hexadecapole contribution will be discussed in 9.2; here we concentrate on the multipoles expansion up to the quadrupole, as that represents the standard analysis. The intermediate panels of Figure 1 show the mean of the mocks using wedges clustering estimator pre-reconstruction (left) and post-reconstruction (right) for 1000 MD-PATCHY for the 3 redshift bins. The analogue plot is shown in Figure 1 bottom panels for ω_ℓ clustering estimator pre/post-reconstruction (left/right panels) for the three redshift bins.

We perform the anisotropic fits following the methodology described in Section 2. We use the sample covariance pre/post-reconstruction for performing the fits computed from the 1000 MD-PATCHY mocks for the different estimators. We show in Figure D1 the respective correlation matrices pre/post-reconstruction for the different estimators: top rows for multipoles estimator; intermediate panels for wedges estimator and bottom panels for ω-estimator (each column represents different redshift bins). The post-reconstruction correlation matrices of multipoles and wedges are clearly more diagonal compared with the pre-reconstructed ones[2].

In Table 3 we present the results for the fiducial methodology using the multipoles. We focus first on the distributions of α and ϵ. The bias column of the table indicates that pre-reconstruction we have $b_\alpha^{\rm pre} = 0.0022 - 0.0042$ and only 0.001 post-reconstruction. For ϵ, we find a bias $b_\epsilon^{\rm pre} \sim 0.001$ remains at the same level except for bin 2 that increases slightly $b_\epsilon^{\rm post} = 0.002$. The standard deviations columns ($S_{\alpha,\epsilon}$) indicates that the dispersion of α and ϵ are reduced post-reconstruction ($S_\alpha^{\rm pre} = 0.0181 - 0.0227$ is reduced to $S_\alpha^{\rm post} = 0.0118 - 0.0136$, $S_\epsilon^{\rm pre} = 0.0227 - 0.0265$ becomes $S_\epsilon^{\rm post} = 0.0132 - 0.0163$). Concerning the error distributions of the fitting parameters, we describe the distributions with the mean and standard deviation, we find that both quantities reduce post-reconstruction. In particular we will just quote the changes on the mean: the mean of the error distribution in α parameter pre-reconstruction $\sigma_\alpha^{\rm pre} = 0.0215 - 0.0262$ reduces to $\sigma_\alpha^{\rm post} = 0.0130 - 0.0147$ post-reconstruction, these results of the mean error are consistent with the dispersions measurements from α and ϵ distributions. For the rest of the paper, when we study variations of the distributions of the best fitting parameters related to the variations in the methodology, instead of referring to the individual distributions of the best fitting results (i.e., $b_\alpha, b_\epsilon, S_\alpha, S_\epsilon, \bar{\sigma_\alpha}, \bar{\sigma_\epsilon}, ...$) we will focus on differences of these variables compared to our fiducial case (i.e., $\Delta\alpha, \Delta\epsilon, \Delta\sigma_\alpha, \Delta\sigma_\epsilon$).

We now move on to discuss the results from using different estimators. As we are interested in measuring the systematic error associated to the estimators, we look at the variations on the mean ($\Delta\alpha, \Delta\epsilon$ defined by Equations 22)[3]. We show the results on Table 4 for quantities pre-/post-reconstruction. Pre-reconstruction we found large differences when using different estimators, further exploration should be done to investigate whether tuning the parameters of the model or using different templates results in a reduction of the differences observed in the distributions of α, ϵ and their uncertainties. Pre-reconstruction correlation function fits are particularly sensitive to the model used in the fits. For the post-reconstruction cases, we find differences $\Delta\alpha < 0.002$ and $\Delta\epsilon < 0.001$ between ω-multipoles estimators for the three redshift bins. For wedges-multipoles the difference in the mean of the best fitting values is $\Delta\alpha, \Delta\epsilon \leqslant 0.001$ for all redshift bins. We report the RMS of the different cases as the error associated to the estimator choice in configuration space.

In addition to our results about two-point estimators in configuration space, we include the results from comparing similar BAO analyses performed with combined sample DR12 (Beutler et al. 2016a; Ross et al. 2016; Alam et al. 2016) to our Configuration Space fiducial methodology denoted ξ_ℓ(V). The results are shown in Table 5. From comparing the multipoles results from Ross et al. (2016) to our fiducial case, we get variations $\Delta\alpha, \Delta\epsilon \leqslant 0.001$ (for more precise figures check numbers in the Table 5). From comparing the multipoles in Fourier Space (Beutler et al. 2016a) (FS) with our Fiducial model we also find variations $\Delta\alpha < 0.001$, but the variations in ϵ are slightly larger ($\Delta\epsilon \leqslant 0.002$). [4]. Finally, we quote the BAO consensus results from Alam et al. (2016) (generated from

[2] We will explore in 6 the effect of reconstruction in the covariance matrices itself and the fits for the multipoles case.

[3] The detailed results of the fits are presented in the Appendix C.

[4] Similar results are found when comparing FS with Ross et al. (2016) results .

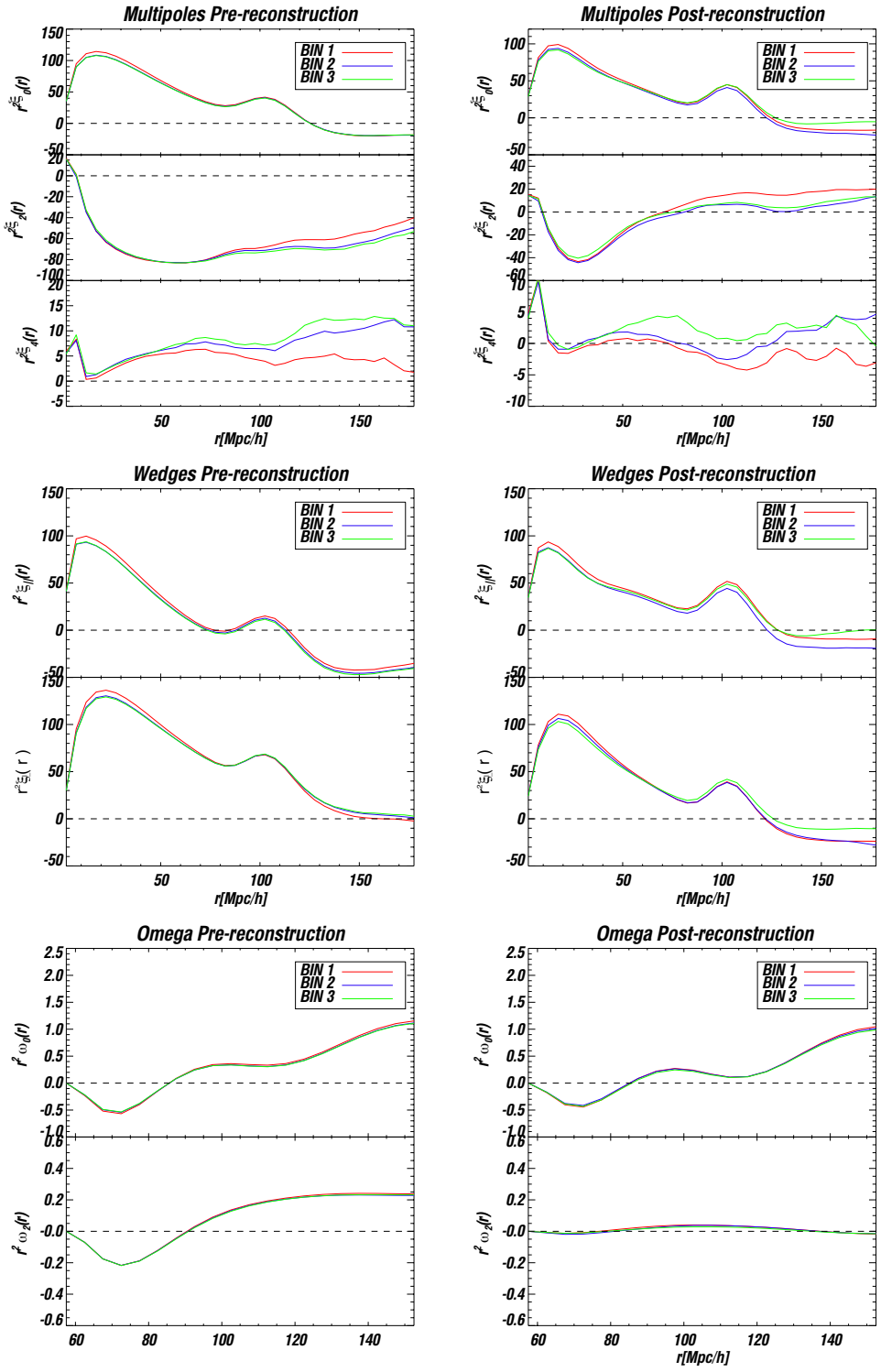

Figure 1. [Top panels Multipoles]. Mean monopole, quadrupole, and hexadecapole from 1000 MD-PATCHY mocks of BOSS COMBINED Samples Pre- (left) and Post-reconstruction (right). [Intermediate Panels] Wedges clustering estimator: Mean of 1000 MD-PATCHY pre-reconstruction (left) and post-reconstruction (right) mocks for the 3 redshift bins. [Bottom Panels] ω_ℓ clustering estimator: Mean of 1000 MD-PATCHY mocks pre-reconstruction (left) and post-reconstruction (right) for the 3 redshift bins.

Table 3. Fitting results from MD-PATCHY mocks (pre) post-reconstruction for the fiducial methodology using multipoles ξ_ℓ (Section 4). The different columns are the mean of the distributions of the best fits parameters and their respective uncertainties denoted by $\bar{x}$, the standard deviation of the distributions , denoted by S_x, the bias defined as the difference of the mean value compared to the expected value for the variable, $b_x = \bar{x} - x_{\rm exp}$, where $x_{\rm exp}$ is the expected value. $\alpha_{\rm exp} = [0.9993, 0.9996, 0.9999]$ and $\epsilon_{\rm exp} = [0.0002, 0.0003, 0.0004]$.

Fiducial Methodology											
DR12 Combined MD-PATCHY mocks, Pre-Reconstruction											
Estimator	$\bar{\alpha}$	S_α	b_α	$\bar{\epsilon}$	S_ϵ	b_ϵ	$<\chi^2/d.o.f.>$	$\bar{\sigma_\alpha}$	S_{σ_α}	$\bar{\sigma_\epsilon}$	S_{σ_ϵ}
Bin 1 ($0.2 < z < 0.5$)	1.0015	0.0227	0.0022	-0.0003	0.0265	-0.0005	29.9/30	0.0262	0.0103	0.0334	0.0135
Bin 2 ($0.4 < z < 0.6$)	1.0038	0.0181	0.0042	0.0014	0.0231	0.0012	29.8/30	0.0222	0.0085	0.0291	0.0119
Bin 3 ($0.5 < z < 0.75$)	1.0039	0.0181	0.0040	0.0003	0.0227	0.0001	29.8/30	0.0215	0.0082	0.0282	0.0119
DR12 Combined MD-PATCHY mocks, Post-Reconstruction											
Bin 1 ($0.2 < z < 0.5$)	0.9986	0.0136	-0.0007	0.0009	0.0163	0.0007	30.6/30	0.0147	0.0067	0.0188	0.0104
Bin 2 ($0.4 < z < 0.6$)	1.0006	0.0118	0.0010	0.0023	0.0132	0.0021	30.9/30	0.0130	0.0058	0.0163	0.0088
Bin 3 ($0.5 < z < 0.75$)	1.0007	0.0121	0.0008	0.0011	0.0138	0.0009	30.6/30	0.0133	0.0052	0.0166	0.0082

Table 4. Estimator Systematic Error. We summarize the variations $\Delta\alpha$, $\Delta\epsilon$ observed from the different estimators. The RMS only considers the wedges and multipoles estimators.

DR12 Pre-Reconstruction						
Est	b_α	b_ϵ	$\Delta\alpha$	$\Delta\epsilon$	$\Delta\sigma_\alpha$	$\Delta\sigma_\epsilon$
Bin 1 ($0.2 < z < 0.5$)						
$\xi_{\parallel,\perp}$	0.0091	0.0079	-0.0069	-0.0084	-0.0014	-0.0078
ω_ℓ	-0.0020	-0.0044	0.0042	0.0039	0.0056	0.0061
Bin 2 ($0.4 < z < 0.6$)						
$\xi_{\parallel,\perp}$	0.0084	0.0065	-0.0042	-0.0053	-0.0015	-0.0084
ω_ℓ	-0.0003	-0.0030	0.0045	0.0041	0.0003	0.0004
Bin 3 ($0.5 < z < 0.75$)						
$\xi_{\parallel,\perp}$	0.0072	0.0077	-0.0032	-0.0076	-0.0006	-0.0081
ω_ℓ	-0.0003	-0.0031	0.0043	0.003	0.0039	0.0038
RMS	-	-	0.0047	0.0057	0.0029	0.0064
	-	-	(0.0050)	(0.0072)	(0.0012)	(0.0081)
DR12 Post-Reconstruction						
Bin 1 ($0.2 < z < 0.5$)						
$\xi_{\parallel,\perp}$	-0.0005	0.0004	-0.0002	0.0003	0.0002	0.0029
ω_ℓ	-0.0026	0.0010	0.0019	-0.0003	0.0025	0.002
Bin 2 ($0.4 < z < 0.6$)						
$\xi_{\parallel,\perp}$	0.0013	0.0031	-0.0003	-0.001	0.0001	-0.0034
ω_ℓ	-0.0004	0.0027	0.0014	-0.0007	<0.0001	-0.0033
Bin 3 ($0.5 < z < 0.75$)						
$\xi_{\parallel,\perp}$	0.0010	0.0015	-0.0002	-0.0006	0.0003	-0.0037
ω_ℓ	-0.0010	0.0007	0.0018	<0.0001	0.0021	0.0014
RMS	-	-	0.0002	0.0007	0.0002	0.0033

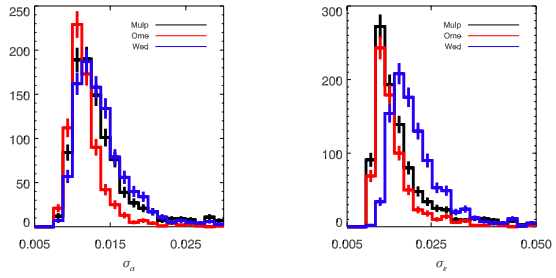

Figure 2. Error Histograms from different clustering estimators $\xi_{0,2}, \xi_{\parallel,\perp}, \omega_l$ for 1000 MD-PATCHY post-reconstruction mocks for the lowest redshift bin. Left panel distribution for σ_α and right panel for σ_ϵ. Similar plots are obtained for the intermediate and higher redshift bins.

Sánchez et al. (2016b) methodology that optimally combines the multipoles in CS and FS) with our fiducial methodology. For the error budget for Alam et al. (2016), we quoted the last one as the systematic error associated to the estimator step, i.e $\Delta\alpha$ =0.0004 and $\Delta\epsilon$ =0.0012 taking the RMS of the three redshift bins.

In addition to the variations in the best fits for α, ϵ for accounting the theoretical systematic error budget, we also analyse the variations in the uncertainties derived from using different estimators; we quote the differences of the mean of the error distributions $\Delta\sigma_\alpha, \Delta\sigma_\epsilon$. The mean differences in the uncertainty, $\Delta\sigma_\alpha$, varies 0.0001–0.0025 between estimators for the post-reconstruction mocks in the three redshift bins. As an illustration of this difference, we show in Figure 2 the error distributions for the first redshift bin using the three different estimators. We observe that the distributions of σ_α for the ω-estimator is narrower with a slightly lower mean error compared with the multipoles errors distribution. The wedges σ_α distribution follows a similar trend to the multipoles. For ϵ, we observe again a slightly narrower distribution for ω-estimator compared with the multipoles; for wedges, error distribution is centred in a larger value compared with the other two distributions. We verified the likelihoods surfaces and 1-d probability distributions in mock-by-mock basis as a sanity check to detect problems on the fits, we found that the larger uncertainties are coming from the wider χ^2 surfaces that generate wider $p(\epsilon)$ dis-

Table 5. Systematic errors from the choice of post-reconstruction estimator, from Alam et al. (2016). We quote $\Delta\alpha$ and $\Delta\epsilon$ (eq.22) over every estimator considered for Alam et. al. (2016) BAO-only. We include the results from using different multipoles analysis in configuration space (this work and Ross et al. 2016 hereafter denoted by $\xi_\ell(R)$). We present also how the multipoles in configuration space (our fiducial methodology) compares to the multipoles in Fourier space using Beutler et al. (2016) hereafter denoted by P_ℓ. Finally, we quoted the differences when using the consensus values from BAO-only (Alam et. al. 2016) methods compares to our fiducial methodology. The RMS is over the consensus lines.

Estimators	b_α	b_ϵ	$\Delta\alpha$	$\Delta\epsilon$
Bin 1 ($0.2 < z < 0.5$)				
ξ_ℓ(V)	-0.0007	0.0007	-	-
$\xi_\ell(R)$	0.0002	0.0009	0.0009	0.0002
P_ℓ	-0.0012	0.0030	-0.0005	0.0023
Consensus*	-0.0008	0.0025	<0.0001	0.0018
Bin 2 ($0.4 < z < 0.6$)				
ξ_ℓ(V)	0.0010	0.0021	-	-
$\xi_\ell(R)$	0.0014	0.0011	0.0004	-0.0009
P_ℓ	0.0005	0.0021	-0.0005	0.0012
Consensus*	0.0008	0.0025	-0.0002	0.0005
Bin 3 ($0.5 < z < 0.75$)				
ξ_ℓ(V)	0.0008	0.0009	-	-
$\xi_\ell(R)$	0.0015	-0.0007	0.0007	-0.0015
P_ℓ	-0.0004	0.0013	-0.0012	0.0006
Consensus*	0.0002	0.0016	-0.0006	0.0008
RMS	-	-	0.0004	0.0012

tributions when marginalising over α. . The fact that the multipoles method should do slightly better than two wedges was shown in Ross et al. (2015). Also it is not surprising that ω-statistic provides smaller errors as it might represent a better compression of the data given that it is less sensitive to nuisance terms in the fitting.

To summarize our systematic errors from BAO distance measurements associated to using different estimators we conclude that $\Delta\alpha < 0.0012$ and $\Delta\epsilon = 0.0006$. However, as in Alam et al. (2016) we are only using multipoles approach (in configuration and Fourier spaces) for getting the consensus values, and as we combined results from multipoles in CS and FS optimally using Sánchez et al. (2016b) methodology, we decide to set the systematic error as the difference between the consensus value and the Fiducial methodology on this paper for consistency with the methodology followed in the paper. Thus the systematic error associated to the estimators to be used in the final error budget is $\Delta\alpha < 0.0004$ and $\Delta\epsilon = 0.0012$.

5 RANDOMS

The computation of 2-point estimators requires the generation of a random set matching the survey geometry and completeness. The error on the correlation function due to the number of randoms is related to the error in the determination of the correlation function for a given sample. In the limit of an infinite random set, the noise contribution from the randoms is zero. However, in practise using a large number of randoms significantly increases the cost of computing the estimator in the analysis. In this section, we test the effect of using different sizes of the random catalogue in anisotropic fits.

Table 6. Fitting results from QPM CMASS mocks Pre/Post-Reconstruction: Random Test (Section 5). The variations in the best fits are defined as: $\Delta\alpha = \alpha_{50\times} - \alpha_{20\times}$ and $\Delta\epsilon = \epsilon_{50\times} - \epsilon_{20\times}$ for pre-reconstruction test. $\Delta\alpha = \alpha_{50\times} - \alpha_{4\times}$ and $\Delta\epsilon = \epsilon_{50x} - \epsilon_{4\times}$ for post-reconstruction test.

Set	$\lvert <\Delta\alpha> \rvert \pm$ RMS	$\lvert <\Delta\epsilon> \rvert \pm$ RMS
CMASS Pre-Rec	0.0008 ± 0.0038	0.0006 ± 0.0066
Bin 1 Post-Rec	0.0002 ± 0.0017	0.0003 ± 0.0035
Bin 2 Post-Rec	0.0002 ± 0.0011	$<0.0001 \pm 0.0015$
Bin 3 Post-Rec	0.0001 ± 0.0015	$<0.0001 \pm 0.0017$
RMS	0.0002	0.0002

For the pre-reconstruction case, the RR and RD pair-counts used in the Landy-Szalay estimator are computed once for all the mocks. The finite size of the randoms coupled with the fact that we use the same random file for all of the mocks is a potential source of scatter that is not in the covariance matrix. We test using two different sets of randoms. If we use a single random catalogue, we might get some small shift that is purely from that random catalogue not being infinite. The difference between that shift and the shift found from a much larger random catalogue should indeed tell you something about the size of the systematic uncertainty.

For the post-reconstruction case the approach is slightly different. In the post-reconstruction case, there are two sets of random catalogues: the denominator randoms used to determine the geometry of the survey, and the numerator randoms that we shift according to the displacement field inferred from data; we call this, shifted random catalogue. The shifted random catalogue is different for every single mock, thus the DS and SS counts need to be recomputed for each mock. From the definition of the Landy-Szalay estimator, we know that the variance in the correlation functions is dominated by the DR paircounts, which goes to as $4/x$ (where x is the ratio of randoms-to-data), with the RR paircounts being subdominant, scaling as $1/x^2$. Thus, if we use $x = 4$ the variance is 10 times bigger than if we use $x = 40$. Thus, we decided to test the effect of the the size of the random catalogues in this case for the SS term for balancing the errors in the correlation function estimate. [5]

5.1 Random size Pre-reconstruction

We test the effect of the randoms pre-reconstruction with 100 QPM CMASS mocks; we use as fiducial cosmology, the natural cosmology of the QPM mocks (see Table 1). We test two random sets: the first case is a random set 20 times the size of the data sample, denoted by "$20\times$", and a second set 50 times the size of the data sample, denoted by "$50\times$". We computed the multipoles using these two set of randoms and then we performed anisotropic analysis described in Section 2. The results are shown in Table 6; we report the mean difference of fits performed on the correlation functions using $20\times$ compared to the correlation functions computed with $50x$ randoms.

[5] In particular, computing the post-reconstruction correlation function requires the computation of very expensive random-random pair-counts for each one of our thousands of mocks catalogues. Thus, this tests is critical for minimizing the computational cost of doing so for 1000 post-reconstruction mocks for the 3 redshift bins.

The main conclusion is that randoms make very small differences in the mean of isotropic/anisotropic fits for both of these two cases. The differences observed are $\leqslant 0.0002$.

5.2 Different number of randoms for DR and RR terms post-reconstruction

We test the effect of the randoms post-reconstruction with 100 QPM CMASS mocks; we use as fiducial cosmology, the natural cosmology of the QPM mocks (see Table 1). We test the effect of randoms differently that pre-reconstruction. We reduce the number of randoms from $50\times$ to $4\times$ for post-reconstruction correlation functions in the numerator SS (not for the SR term) and we test the impact on the fitting parameters. We show the results in table 6 of the best fits distributions obtained with 100 mock catalogues. The differences between the $50\times$ and the $4\times$ anisotropic fits are very small: 0.0002 for α and 0.0002 for ϵ. The variations in the anisotropic fits when using different numbers of randoms must be random (i.e., not systematic); these variations must be statistical fluctuations and they should be in our covariance matrices if we use the same numbers of randoms. However, the finite size of the randoms is a potential source of scatter that is not in the covariance matrix, and what are demonstrating is that it is not contributing significantly to the scatter.

As an additional output of this test, the results validate the use $50\times$ pair-counts for DS pair-counts and $7x$ for SS for the mock covariance for Alam et al. (2016). With the current 2-point correlation code and the number of mocks required for doing BAO/RSD analysis using the correlation function, a total of 132,000 CPU-hours were required for estimating the post-reconstruction pair counts using EDISON at NERSC. DR12 correlation functions were computed with $50\times$ randoms pre and post-reconstruction.

We conclude that there is no systematic error in BAO distance measurements associated to the number of randoms. The variations in the scatter are < 0.0001 in α and ϵ.

6 COVARIANCES

The covariance matrix, in particular its inverse, is crucial for obtaining the cosmological parameters from the galaxy surveys (Percival et al. 2014). The usual way to get the covariance matrix is to use the brute force approach, which consists of using a large number of mock catalogues to estimate the sample covariance matrix. For the analysis of BOSS two sets of mock catalogues were considered, QPM and MD-PATCHY. Different methods were used to generate these sets of mocks, and so we test the systematic consequences of using the corresponding covariance matrices for BAO fitting.

New approaches have been proposed in the existing literature to avoid using mock catalogues given their computational cost (Pope & Szapudi 2008; de la Torre & Peacock 2013; Paz & Sánchez 2015; Schneider et al. 2011; O'Connell et al. 2015). In addition to the testing different sets of mocks, we tested the theoretical approach developed by O'Connell et al. (2015) based on a Gaussian model were few parameters are calibrated with the simulations.

In 6.1 we discuss general differences between the (inverse) covariance matrices provided by the QPM and MD-PATCHY mocks. In 6.2 we discuss the model covariance matrix and compare its general features to the mock covariance matrices. In 6.3 we present the results of using each matrix for non-linear BAO fitting. Throughout this section the fiducial choice for the covariance matrix is the sample covariance obtained from the PATCHY mocks.

6.1 Comparison of Sample Covariance Matrix in DR12

We analyze the sample covariances generated from two sets of DR12 mock catalogues: QPM and MD-PATCHY[6]. We separate the analysis in two different aspects: 1) Sample Covariance differences related to reconstruction, 2) Sample Covariance differences related to different mock catalogues. We study how the structure of the covariance matrix changes between different cases (pre- vs post-reconstruction mocks and QPM vs MD-PATCHY mocks) and how these differences reflects on the anisotropic fits. For the comparisons we chose to work with the inverse of the covariance matrix, i.e., the precision matrix. The main reason is that it is the precision matrix which is used directly in the fitting process, and the mapping between the covariance matrix and its inverse is highly non-linear. An additional advantage of working with the precision matrices is that the structure of the precision matrix is simpler, thus it is easier to determine the similarity/discrepancies in the matrices.

In order to make plots of the precision matrices easier to read, we provide a discussion of the general features of the precision matrices considered in this paper. As is readily seen in Figure 3, the structure of the precision matrix is primarily (but not exclusively) concentrated on the diagonal and first off-diagonal of the matrix. The naive r-dependence of these diagonal contributions is $\Psi_{ab} \sim r_a r_b$, and so throughout this section we will plot $\Psi_{ab}/r_a r_b$. This rescaling is applied to the middle plot in Figure 3, which illustrates that this removes most (but not all) of the r-dependence from the plot. The middle plot also indicates that our measurements of the monopole (lower left) are significantly more precise than our measurements of the quadrupole (upper right). We can compensate for this be dividing the quadrupole by a compensating factor of $\sqrt{4.7}$, then propagating this rescaling through to the precision matrix. The result, shown in the rightmost plot in Figure 3, is that we can see that the precision for the quadrupole has essentially the same structure as the precision for the monopole, and that after these rescalings the noise on the precision matrix is approximately homogeneous. We can also assess the significance of the monopole-quadrupole terms, relative to the monopole-monopole and quadrupole-quadrupole terms. In all of these plots a sharp decline in precision is observed for the bins with smallest and largest r. This arises because these are the smallest/largest bins that we consider, and does not indicate anything else unusual about those bins.

Before assessing the detailed structure of the various precision matrices, we consider whether any of these matrices are, in total, "more precise" than any of the others. We do this comparison by evaluating $\log(\det(\Psi))$, which captures the overall amplitude, on each matrix. In order to facilitate comparison between each matrix and the fiducial case (post-reconstruction Patchy mocks), we also calculate the overall rescaling that would have to be applied to the *fiducial* matrix in order to make its amplitude match that of each other case. We report these as percent changes, with negative values indicating that the matrix is *less* precise than the fiducial case, and positive values indicating that the matrix is *more* precise than the fiducial case. We discuss this table in the following subsections.

[6] We test in the Appendix B how the covariance generated with previous generation of mock catalogues (PTHALOS) compares with one generated with the new sets of mock catalogues available (QPM).

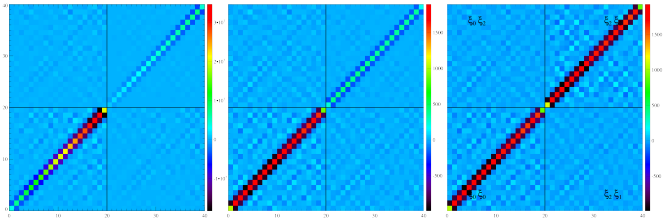

Figure 3. Precision matrix for the post-reconstruction Patchy mocks (bin 2) with different scalings. On the left, the precision matrix with no rescaling applied. It illustrates that the bulk of the structure in the precision matrix is on the diagonal and first off-diagonal. In the middle, we divide out the naive scaling with r and plot $\Psi_{ab}/r_a r_b$.This illustrates that the naive scaling largely captures the r-dependence of the precision matrix. On the right, we apply the radial scaling and scale up the quadrupole by a factor chosen to put the monopole and quadrupole on equal footing, which helps assess the amplitude of the main monopole-quadrupole entries.

Table 7. Evaluation of $\log(\det(\Psi))$ for each matrix. This quantity captures the overall amplitude of each matrix i.e. facilitate the comparison between each matrix and the fiducial case (post-reconstruction Patchy mocks). We also calculate the overall rescaling that would have to be applied to the *fiducial* matrix in order to make its amplitude match that of each other case. We report these as percent changes, with negative values indicating that the matrix is *less* precise than the fiducial case, and positive values indicating that the matrix is *more* precise than the fiducial case.

Values of $\log(\det(\Psi))$		
Mocks	$\log(\det(\Psi))$	Percent change
Bin 1 ($0.20 < z < 0.50$)		
QPM, pre-reconstruction, bin 1	594.2	-7.6%
Patchy, pre-reconstruction, bin 1	588.2	-19.0%
QPM, post-reconstruction, bin 1	600.5	+8.1%
Patchy, post-reconstruction, bin 1	597.1	-
Model, bin 1	597.1	-0.7%
Bin 2 ($0.40 < z < 0.60$)		
QPM, pre-reconstruction, bin 2	601.9	-10.1%
Patchy, pre-reconstruction, bin 2	598.0	-16.8%
QPM, post-reconstruction, bin 2	607.8	+4.1%
Patchy, post-reconstruction, bin 2	606.1	-
Model, bin 2	605.8	-0.9%
Bin 3 ($0.50 < z < 0.75$)		
QPM, pre-reconstruction, bin 3	586.2	-11.6%
Patchy, pre-reconstruction, bin 3	585.0	-12.8%
QPM, post-reconstruction, bin 3	591.5	+0.9%
Patchy, post-reconstruction, bin 3	591.1	-
Model, bin 3	591.2	+0.3%

6.1.1 Pre/Post-reconstruction Covariances

The first question we address is if what are the effects of reconstruction on the precision matrix. In Figure 4 we show the precision matrix for the MD-PATCHY mocks. On the first row the pre-reconstruction precision matrix obtained for the 3 redshift bins: low, intermediate, and high redshift bin (from left to right). In the second row, the post-reconstruction precision matrix for the corresponding redshift bins. In the third row the difference between post- and pre-reconstruction precision matrices. From the third row we notice different trend for the three redshift bins,

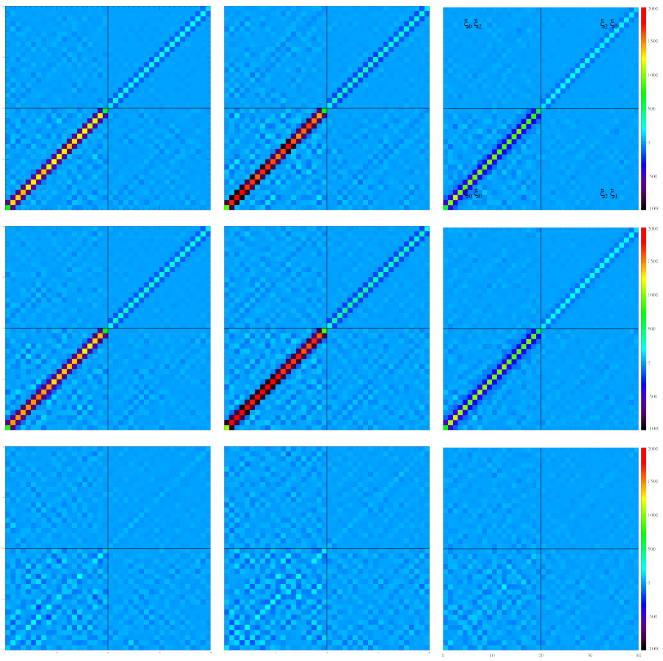

Figure 4. Precision matrix for 1000 MD-PATCHY mocks. On the first row the pre-reconstruction precision matrix obtained for the 3 redshift bins: low, intermediate, and high redshift bin (from left to right). In the second row, the post-reconstruction precision matrix for the corresponding redshift bins. In the third row the difference between post- and pre-reconstruction precision matrices.

the higher redshift bin shows smaller differences compared to the lower and intermediate bins. We observe that the differences in the precision matrices pre-reconstruction are concentrated in the diagonal terms of the monopole-monopole, quadrupole-quadrupole, monopole-quadrupole; everywhere else we find a noise pattern indicating the consistency between precision matrices. The noise level seems equivalent for pre and post-reconstruction precision matrices.

In table 7 we quantify the overall rescaling of the precision matrix required to make the values of $\log(\det(\Psi))$ match. We observe a $\sim$16% increase in the precision post-reconstruction for the PATCHY mocks (taking the RMS of the three redshift bins), and a $\sim$ 14% increase in precision for the QPM mocks. The increase in precision post-reconstruction for both QPM and Patchy mocks likely results from the effects of reconstruction on the higher-point correlation functions, since reconstruction has little impact on the overall amplitude of the 2-point correlation function or the survey volume, and those together determine the Gaussian contributions to the covariance matrix.. Patchy improves more than QPM, although post-reconstruction they have similar values.

We show in the left panel of Figure 5 the diagonal terms of the precision matrices for the three redshift bins for MD-PATCHY. In the right panel, we show the off-diagonal terms of the precision matrices for the same three redshift bins. The top panels correspond to the monopole terms and the bottom ones to the quadrupole terms. There is a re-scaling by r^2 to eliminate radial trends. As stated above the precision matrices are approximately uniform across r, once the $r_a \times r_b$ scaling is taken into account. In these plots we can see by eye the slight residual r-dependence. It also appears that the improvement in precision from reconstruction is localized to the diagonal bins, as the off-diagonal bins are largely unchanged.

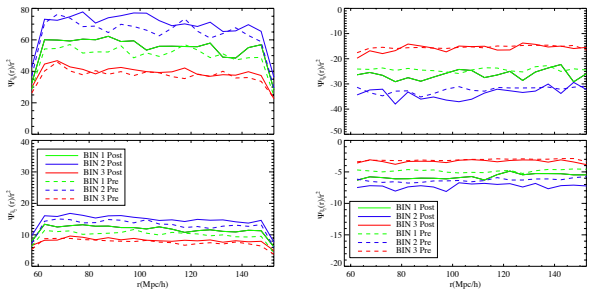

Figure 5. Diagonal [left] and Off-Diagonal [right] terms of Precision Matrices of MD-PATCHY for 1000 mocks for the 3 redshift bins, Pre/Post-reconstruction. Top panels Monopole terms, bottom panels quadrupole terms.

For the fitting results, we quantify how much of the improvement in the best fitting parameters and their uncertainties comes from the differences in covariance and how much comes from the reconstruction of the sample. In Table C2 we show the results of performing the BAO anisotropic analysis to the 1000 PATCHY/QPM mocks using the different covariances. We study first the bias associated with the α measurements for MD-PATCHY: b_α reduces post-reconstruction as expected from 0.002 to $<$0.001 for the lower redshift bin, 0.004 to 0.001 for the intermediate and higher redshift. QPM bias shows no reduction of the shift post reconstruction for the lower bin (0.003 for both cases), the intermediate bin decreases from 0.005 to 0.001 and for the higher redshift bin 0.003 to 0.001. The results post reconstruction for the bias are in agreement for both mock catalogues except for the lowest redshift bin. Comparing the post-reconstruction results using post-reconstruction covariances against the post-reconstruction results using pre-reconstruction covariances, we observe, as expected, that the decrease in the error bars also is mostly related to the reconstruction of the catalogue and not to the covariance changes post-reconstruction. The decrease in the mean error distributions obtained from analyzing post reconstruction catalogues compared from their value pre-reconstruction is 0.011 for α and 0.015 for ϵ for the first redshift bin. The difference when instead of the post-reconstruction covariance, we use the pre-reconstruction covariance is only 0.004 for both α and 0.007 for both ϵ; similar numbers result out from analyzing the intermediate and higher redshift bins. The differences in the standard deviation are ΔS_α between pre and post reconstruction distributions are 0.006-0.009, and the differences in the dispersion when we use the covariance pre-reconstruction for fitting the post-reconstruction correlation functions is 0.001-0.005. Indicating again that the post-reconstruction covariance also is contributing to the reduction of the dispersion on the fits. Finally we move on to the uncertainties, the reduction of the mean uncertainties when comparing pre and post-reconstruction results is 38-44% for α and ϵ, when we compared the error distributions using the covariance pre-reconstruction (instead of the post-reconstruction) in the post-reconstruction fits the improvement is only 24-31%, the reduction of the errors observed is coming exclusively from the covariance post-reconstruction. However, the impact is mostly in the dispersion of the uncertainties distributions; using the post-reconstruction covariance, these are narrower compared to the pre-reconstruction ones. The dispersion reduces from pre-reconstruction to post-reconstruction in 31-36% and when we use pre-reconstruction covariance instead for the fits the reduction is only 20-28%, again the difference in the dispersion is related only to the use of the post-reconstruction covariance matrix.

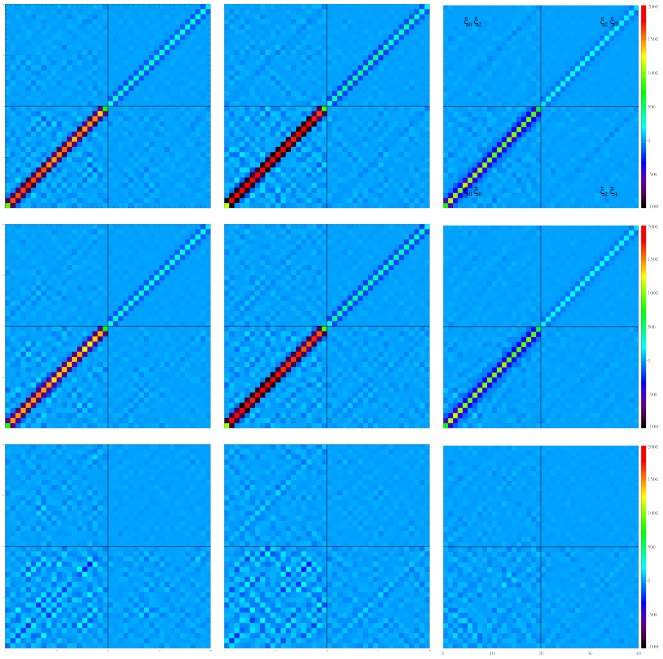

Figure 6. Difference between precision matrix of 1000 from PATCHY mocks and QPM mocks for the 3 redshift bins, Pre-reconstruction (top) and Post-reconstruction (Bottom). The differences are re-scaled by r^2. Each precision matrix has four blocks bottom left is the monopole-monopole term, top-right the quadrupole-quadrupole and bottom-right and top-left the cross-terms.

6.1.2 *Differences in Sample Covariances from different mock catalogues*

In this section we check if there are differences in the structure of the sample covariance matrices generated from different sets of mock catalogues: QPM and MD-PATCHY. We then quantify if these differences have a significant effect on the fitting results and the uncertainties. We proceed to analyze only the post-reconstruction results as for the BAO analysis, the covariance used is always post-reconstruction.

In Figure 6 we show the precision matrix for the MD-PATCHY different sets of mocks post-reconstruction, top [PATCHY] and intermediate panels [QPM]; bottom panels, we show the difference between the precision matrix generated from PATCHY and the precision matrix generated from QPM for the three redshift bins, low, intermediate and higher redshift bins, respectively.

We notice different trend for the three redshift bins, the higher redshift bin (earliest time) shows that QPM and PATCHY are completely consistent , while lower and intermediate bins shows differences. We observe a similar trend in the $\log(\det(\Psi))$, the values are pretty similar for the high redshift bin (earliest time) between QPM and PATCHY, then grow in bin 2 and grow further in bin 1. We speculate that this behaviour may result from QPM developing non-Gaussian structure less rapidly than Patchy, but further exploration would be required to verify this hypothesis.

In the left panel of Figure 7, we see the diagonal terms of the precision matrices for the three redshift bins in different

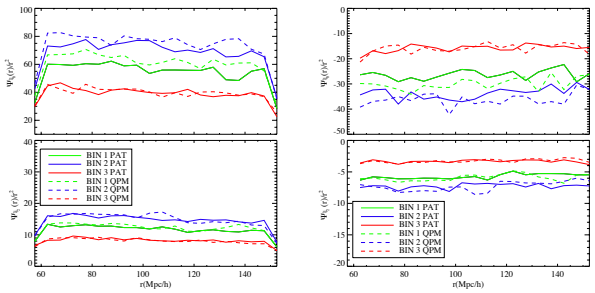

Figure 7. Diagonal [left] and Off-Diagonal [right] terms of Precision Matrices of QPM and MD-PATCHY for 1000 mocks for the 3 redshift bins, Post-reconstruction. Top panels Monopole terms, bottom panels quadrupole terms.

colours for both sets of mock catalogues: QPM [dashed lines] and MD-PATCHY [solid lines]. In the right panel, we see the off-diagonal terms of the precision matrices for the same three redshift bins for both sets of mocks catalogues. Top panels again refer to the monopole terms and bottom ones to the quadrupole terms. The values of the precision are re-scaled to remove the naive r-dependence. In contrast to the pre/post-reconstruction comparison, we see clear differences in both the diagonal and off-diagonal plots. The diagonal terms of the precision matrix for QPM mocks shows slightly larger values (10-20%) in the monopole terms, for the quadrupole the variations are smaller ($\sim$ 10%). For the off-diagonal terms, the QPM monopole terms are $\sim$ 20% smaller, for the quadruple terms we observe 20% variations, showing again QPM smaller values than MD-PATCHY.

In Table C3 we show the results of performing the BAO anisotropic analysis on the 1000 mocks using the different covariances. Regarding the best fitting parameters, first we verify the bias column , the different covariances provides unbiased estimates of the parameters α and ϵ, the mean bias are for the most of the mocks is $b_\alpha \sim 0.001$ and $b_\epsilon = 0.001 - 0.002$ for MD-PATCHY and $b_\epsilon = 0.003 - 0.004$ for QPM. The dispersion is very similar for both mock catalogues. We also find differences in the dispersion of α and ϵ distributions ($\Delta S_\alpha = 0.001 - 0.002$, $\Delta S_\epsilon < 0.001$)

The error distributions are also very similar; we find differences in the mean values between 0.001-0.002 for σ_α and σ_ϵ. Additionally the dispersion of the error distributions shows variations of the same order.

We also tested the BAO fitting methodology on one set of mocks using the covariance given for the second set of mocks to quantify how the best fitting parameters could be affected by using a covariance matrix derived from a different set of mocks. The variations in the best fitting parameters are around 0.001 for α and ϵ for the three redshift bins as well as the differences on the mean values of the uncertainties distributions. The dispersion also shows variations of the same order for α. Finally we proceed to quantify the differences in the mean of α and ϵ distributions. For α we found the low redshift bin differs between mock sets by 0.0003-0.0005, while the intermediate and high redshift bins shows 0.0013-0.0017 and 0.0002-0.0005.

6.2 Comparison between Sample and Theoretical covariance

The second kind of covariances we want to test against the fiducial choice is using semi-analytic models for the covariance matrix. We tested the theoretical approach proceed by O'Connell et al. (2015) based on a Gaussian model were two parameters (shot noise and volume) are calibrated with the mock catalogues. Testing hybrid methods for generating covariance matrices will be important in the context of future surveys as we will need to apply hybrid methods for the large scale structure analysis given the increasing quantity of data and volumes that increase the computation requirements for the estimation of the covariances in the large scale structure analysis.

6.2.1 Model Covariance Matrix for DR12

The approach in O'Connell et al. (2015) makes a few simplifying assumptions in order to produce a tractable, realistic model for the covariance matrix. Most importantly, the galaxy field is assumed to be Gaussian. For a Gaussian random field, the covariance of the two-point correlation function can be written in terms of integrals of the four-point correlation function. Gaussianity implies that the four point correlation function has no connected piece, and can be written entirely in terms of the two-point correlation function.

We then assume that the galaxy survey is a Poisson-sampled version of the underlying galaxy field. The covariance of the two-point function in the galaxy survey is then a sum of integrals over configurations of two, three, and four points. Since the underlying field is still assumed to be Gaussian, the integrands are composed only of the underlying two-point correlation function and the number density. A key innovation of O'Connell et al. (2015) is to allow the number density to vary, incorporating both the position-dependent survey mask and redshift-dependent number density of galaxies. The resulting integrals must be performed numerically, but are found to converge quite efficiently. The estimates below used $\approx$ 600 CPU hours for each redshift bin.

The galaxy field is known to be non-Gaussian, and O'Connell et al. (2015) saw clear evidence of the effects of non-Gaussianity on the covariance matrix. The technique introduced there to model the effects of non-Gaussianity is simply to increase the level of shot noise in the survey. The intuition behind this is simple – the 3- and 4-point functions primarily affect the galaxy field at relatively short scales, which are also where the effects of shot noise are most relevant. The shot noise re-scaling is implemented as an overall re-scaling of the 2-, 3-, and 4-point integrals. The fitting is performed using a likelihood function based on the Kullback-Leibler divergence introduced in O'Connell et al. (2015) , where it was shown that the shot-noise rescaling could be determined using a small number of mocks. Here, since our goal is simply to construct a usable model, the shot noise was determined using the full suite of 1,000 MD-PATCHY mocks.

The implementation of the described method for this study differs slightly from the implementation in (O'Connell et al. 2015). First, the present analysis utilises a monopole-quadrupole decomposition of the correlation function rather than evaluating the correlation function in $r - \mu$ bins. To accommodate this, the covariance matrix was determined using 20 μ bins, then projected down to the monopole+quadrupole covariance matrix. This projection was performed separately for the 2-, 3-, and 4-point contributions to the covariance matrix, before fitting the shot-noise re-scaling.

Second, the present analysis combines counts of galaxies in the North and South galactic caps (NGC and SGC), since the survey masks and redshift-dependent number densities used to compute the model covariance matrix are different in the NGC and SGC. The 2-, 3-, and 4-point contributions to the covariance matrix from the NGC and SGC were computed separately and then combined, again prior to fitting of the shot-noise re-scaling. The estimates of

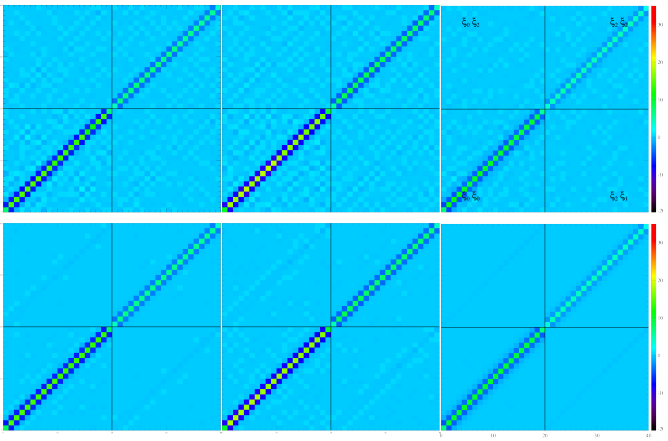

Figure 8. Precision Matrices of MD-PATCHY for 1000 mocks [top panels] and model precision matrices [bottom panels] for the 3 redshift bins, Post-reconstruction.

the random-random pair counts in each galactic cap were used to determine the relative weight given to each cap. Specifically, the combination was performed as

$$C_{\rm comb} = \frac{{\rm mean}(RR_{\rm NGC})}{{\rm mean}(RR_{\rm NGC}+RR_{\rm SGC})}C_{\rm NGC}+ \\ +\frac{{\rm mean}(RR_{\rm SGC})}{{\rm mean}(RR_{\rm NGC}+RR_{\rm SGC})}C_{\rm SGC}\,.$$

Third, in addition to allowing the shot-noise re-scaling to vary in the fitting, the overall survey volume is also a free parameter. This was done to accommodate minor differences between the volume and number density described by the survey mask and observed redshift-dependent galaxy number density, and the volume and number density implemented in the mocks. Minor discrepancies between the two can arise e.g. from survey defects, such as bright stars, that are accounted for in the mocks but that are too small to be accurately reflected in the survey mask.

6.2.2 Results from Model Covariance

First, we compare the structure of the sample precision matrix estimated from mock catalogues to the model precision matrix. The comparison between precision matrices is shown in Figure 8. The top panels are the precision matrix for the three redshift bins from MD-PATCHY mock catalogues; the lower panels are from model covariance. The most noticeable aspect is the clear noise reduction of the model covariance compared with the sample covariance from a finite number of mocks.

We show in the left panel of Figure 9 the diagonal terms of the precision matrices for the three redshift bins for the model covariance and the sample covariance computed from MD-PATCHY mock catalogues. In the right panel, the off-diagonal terms of the covariance matrices for the same three redshift bins. The top panels correspond to the monopole terms and the bottom to the quadrupole terms. There is a re-scaling by the $r_a \times r_b$ to remove the naive scaling with r. We observe again this clear reduction in the noise comparing the noisy estimate from sample covariance with the smooth line coming from model covariance. The diagonal terms for the monopole are almost identical in sample and model precision matrices. The quadrupole diagonal terms for the sample covariance are slightly larger than the model covariance. For the off-diagonal

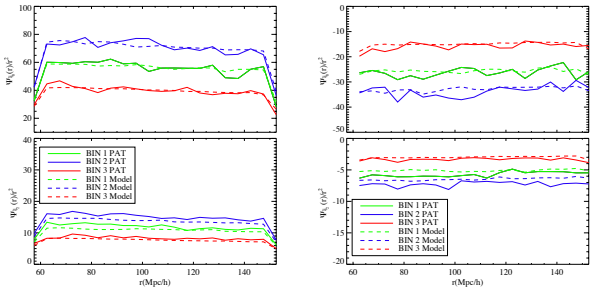

Figure 9. Diagonal and Off-Diagonal terms of Model and Sample Precision Matrices of MD-PATCHY for 1000 mocks for the 3 redshift bins, Post-reconstruction.

terms we have similar trend , the monopole terms are very similar, and the quadrupole terms show slightly larger variations; the sample covariance having more negative values. Comparing the values of $\log(\det(\psi))$ in Table 7 we observe the re-scaling between the sample covariance from PATCHY and model covariance are very small compared with the other cases showing the model is in exceedingly good agreement with post-reconstruction Patchy as expected as it has been fit to post-reconstruction Patchy.

The excellent agreement between the mock and model precision matrices indicates that, for future surveys, better-understood and more realistic mocks should be a higher priority than generating large numbers of mocks. This follows from the simple observation that the differences between the QPM and MD-PATCHY mock covariance matrices are larger than the differences between the MD-PATCHY mock covariance and the model covariance, produced as in O'Connell et al. (2015) and fit to the MD-PATCHY mock covariance.

Secondly, we analyze the performance of the model covariance compared with the sample covariance in term of anisotropic fits. Table C3 summarizes the results of performing the BAO anisotropic analysis on the 1000 MD-PATCHY mocks using the model and sample covariances. The distributions of best fitting parameters as well as the error distributions are extremely similar: the bias for all cases are $b_\alpha, b_\epsilon \sim 1$. The dispersion of α and ϵ distributions differs by less than 0.001

The differences in the mean uncertainties and the differences in their dispersion for all the redshift bins are also $\sim$0.001. Finally the differences between the means of the fits using model covariance matrix compared to the fiducial covariance matrix are $\Delta\alpha = (0.0002, 0.0005, 0.0003)$ and $\Delta\epsilon = (< 0.0001, 0.0007, 0.0008)$.

6.3 Summary for Covariances-Systematic Uncertainty

To finish this section we want to give an estimate of the systematic error associated to the covariance step in the BAO analysis. From Table C2 we have nine estimates for the variation in α, ϵ parameters for different choices of covariance matrices, we compute those differences and we present them in Table 8. We will generate a final estimate of the systematic uncertainty from the RMS of the nine values. We decided to not include the differences coming from the model covariance cases as the variations are very small and they will artificially decrease the error estimate.

Summarizing the covariance results we found that using different mock catalogues produces variations in the best fits 0.0002-0.0017 in α and 0.0002-0.0013 in ϵ. The variations between model and sample found are lower than 0.0010. We conclude that the sys-

Table 8. Covariance Matrix Systematics. We summarize the variations $\Delta\alpha, \Delta\epsilon$ observed from the different combinations from Table C2. *The PP-model cases are not take into account in the RMS calculation because are too small.

DR12 Sample Covariance Pre-Reconstruction				
Cov	$\Delta\alpha$	$\Delta\epsilon$	$\Delta\sigma_\alpha$	$\Delta\sigma_\epsilon$
Bin 1 ($0.20 < z < 0.50$)				
PP-QQ	-0.0012	-0.0031	0.0038	0.0014
Bin 2 ($0.40 < z < 0.60$)				
PP-QQ	-0.0002	-0.0021	0.0024	0.0011
Bin 3 ($0.50 < z < 0.75$)				
PP-QQ	0.0008	-0.0035	0.0017	0.0002
RMS	0.0008	0.0030	0.0028	0.0010
DR12 Sample Covariance Post-Reconstruction				
Cov	$\Delta\alpha$	$\Delta\epsilon$	$\Delta\sigma_\alpha$	$\Delta\sigma_\epsilon$
Bin 1 ($0.20 < z < 0.50$)				
PP-PQ	-0.0003	0.0002	0.0009	0.0014
QQ-QP	-0.0005	0.0004	-0.0008	-0.0019
PP-model*	-0.0002	<0.0001	0.0003	-0.0002
Bin 2 ($0.40 < z < 0.60$)				
PP-PQ	0.0017	0.0013	0.0002	0.0007
QQ-QP	-0.0013	-0.0006	0.0001	-0.0005
PP-model*	0.0005	0.0007	<0.0001	-0.0008
Bin 3 ($0.50 < z < 0.75$)				
PP-PQ	0.0002	0.0011	-0.0004	0.0003
QQ-QP	0.0005	-0.0013	0.0002	-0.0002
PP-model*	-0.0005	0.0008	<0.0001	<0.0001
RMS	0.0009	0.0009	0.0005	0.0010

tematic error in BAO distance measurements associated to using different techniques for estimating the covariance matrix is 0.0009 for α and 0.0009 for ϵ, from taking the RMS of all the combinations analyzed in this section. The differences in the uncertainties distributions are $\Delta\sigma_\alpha$ =0.0005 and $\Delta\sigma_\epsilon$ =0.0010.

7 RECONSTRUCTION

There are numerous works which have looked into different sources of systematics error related with the reconstruction algorithm, especially within the BOSS collaboration. We refer the reader to these reconstruction related systematics studies (Padmanabhan & White 2009; Seo et al. 2010; Burden et al. 2014; Vargas-Magana et al. 2014; Burden et al. 2015; Vargas-Magana et al. 2015; Seo et al. 2016). In this work, we devoted two sections (this section and Section 8) to study systematic errors related with reconstruction. This section is devoted to revisit the effect of smoothing scale used on reconstruction of the density field, in the anisotropic BAO parameters. Section 8 test the effect of using different fiducial cosmology, including the effects related with reconstruction. New potential systematics related to reconstruction are explored in Vargas-Magana et al. in prep, where we study the effects on anisotropic BAO fits from redshift distortions corrections in Fourier space reconstruction.

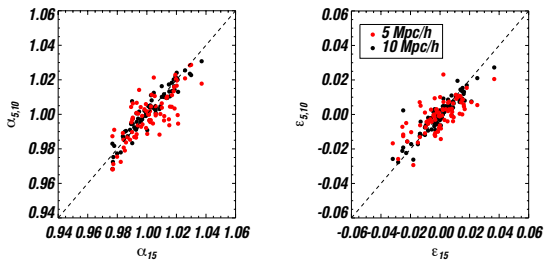

Figure 10. Dispersion plots of best fits from different smoothing scales 5,10 h^{-1}Mpc for 100 MD-PATCHY post-reconstruction mocks for the intermediate redshift bin. Left panel dispersion plots for α and right panel for ϵ.

Previous results are summarized in Table 9. Burden et al. (2014) have studied the effect on smoothing scale when performing isotropic fits to the power spectrum monopole. They found variations in the $\alpha \leqslant 0.001$ when testing the smoothing scale using PTHALOS mocks, the precise numbers for the differences in best fits parameters between the smoothing scales tested are enumerated in Table 9. Vargas-Magana et al. (2015) extended the study to anisotropic BAO analysis and found the variations are between 0.004-0.005. The test were performed with different simulations, QPM mocks and also using different reconstruction implementations (Vargas-Magana et al. 2015; Padmanabhan et al. 2012). The specific numbers for the different smoothing scales and reconstruction implementations are enumerated in the Table 9. Given the differences in the systematic bias found in previous studies, in this section we revisit previous results related to the effect of smoothing scale in the anisotropic BAO parameters in the context of Combined Sample and using a different set of mocks MD-PATCHY.

We performed reconstruction over 100 MD-Patchy mocks for Bin 2 of Combined sample, we used a bias $b = 2.1$ and growth factor $f = \Omega_m^\gamma$ for the fiducial values and γ value for General Relativity. We use three different smoothing scales 5,10,15 h^{-1}Mpc. We compute the multipoles and we performed the fits using fiducial methodology (Table 2). We present the results in Table C6. We use the covariance matrix from the 1000 mocks to prevent that the noise in the covariance generates large fluctuations in the best fitting values. This approximation neglects the impact of the smoothing scale on the covariance matrix properties. However, we experimented fitting the mocks using the noisy covariance matrix generated from the 100 mocks and we find very large bias in the distributions. Thus we decided to fix the covariance for all the cases to the one generated from 1000 mocks and 15 h^{-1}Mpc smoothing scale.

We present in Figure 10 the dispersion plots from comparing the fiducial case (15 h^{-1}Mpc) with the two variants (5,10 h^{-1}Mpc), we observed the values are well correlated for the three cases indicating there are no issues with the fits. The bias measured in the best fits values for the three cases are very small < 0.002 for α and < 0.001 for ϵ. Finally to obtain the systematic error associated to reconstruction, in particular related to the smoothing scale, we compute the variations in the best fit parameter related to this step, the values are shown in Table 10. We quoted the RMS of the two combinations that will serve as our systematic error associated to the reconstruction variations tested in this work.

We conclude that the systematic error in BAO distance mea-

Table 9. Reconstruction related systematics: variations in anisotropic BAO parameters for different smoothing scales (R). We present the results from previous works. We quote the $\Delta\alpha$ and $\Delta\epsilon$ (eq.22) given by the differences between the fiducial smoothing scale 15 h^{-1}Mpc and the variant of the smoothing scale being tested.

Mocks	Sample	R	Reconstruction Implementation	Reference	$\Delta\alpha$	$\Delta\epsilon$
QPM(200)	CMASS	5	Vargas FS	Vargas-Magana et al. (2015)	0.005	0.001
QPM(200)	CMASS	10	Vargas FS	Vargas-Magana et al. (2015)	0.004	<0.001
PTHALOS(600)	CMASS	5	Burden FS	Burden et al. (2014)[7]	<0.001	-
PTHALOS(600)	CMASS	10	Burden FS	Burden et al. (2014)	0.001	-

Table 10. Reconstruction related systematics: variations in anisotropic BAO parameters for different smoothing scales. We quote the $\Delta\alpha$ and $\Delta\epsilon$ (eq.22) given by the differences between the fiducial smoothing scale 15 h^{-1}Mpc and the variant of the smoothing scale being tested. We use 100 mocks PATCHY mocks for the intermediate redshift bin. The also include the RMS of the $\Delta\alpha$ and $\Delta\epsilon$ considering the two smoothing scales tested.

Mocks	R	b_α	b_ϵ	$\Delta\alpha$	$\Delta\epsilon$
PATCHY(100)	5	0.0033	-0.0006	0.0022	0.0009
PATCHY(100)	10	0.0024	-0.0004	0.0009	0.0002
RMS				0.0017	0.0006

surements associated to the smoothing scale used in reconstruction of the density field 0.0017 for α and 0.0006 for ϵ.

8 FIDUCIAL COSMOLOGY ASSUMED IN THE ANALYSIS

The cosmology affects three stages of the analysis: first, the comoving coordinate calculation; second, the fitting template, and third, the cosmological parameters assumed in reconstruction. We test in this section the effect of the three stages together instead of studying the individual contributions at each stage as we wanted to study the overall effect on the best fits. Previous works have explored the dependency on cosmology in the fitting template and reported variations of $\Delta\alpha < 0.001$[8] (Xu et al. (2012b)), test over the distance-redshift relation and test varying the cosmological parameters are not reported in previous works. In order to study the fiducial cosmology dependence of BAO anisotropic analysis, we analyze QPM mocks assuming a fiducial cosmology different from the one used to generate the mocks. We perform the anisotropic BAO analysis and compare to the results when we assume the "true" cosmology. The fiducial cosmologies used for analyzing the QPM mocks are summarized in Table 11. Anderson is a flat cosmology that is shifted in Ω_m by 0.5% compared to QPM cosmology, but have exactly the same Ω_b, h.

We estimate the mean shift that we should observe in the fitted parameters due to the fact that we are using the wrong cosmology. The shifts in α and ϵ are given by:

$$\alpha = \frac{D_{V,\rm fid}}{D_{V,\rm true}}\frac{r_s^{\rm true}}{r_s^{\rm fid}} = \left[\frac{(D_A^{\rm fid}(z))^2 H^{\rm true}(z)}{(D_A^{\rm true}(z))^2 H^{\rm fid}(z)}\right]^{1/3}\frac{r_s^{\rm true}}{r_s^{\rm fid}}, \quad (23)$$

$$\epsilon = \left[\frac{H^{\rm true}(z) D_A^{\rm true}(z)}{H^{\rm fid}(z) D_A^{\rm fid}(z)}\right]^{1/3} - 1. \quad (24)$$

[8] The fits were performed with 15% larger Ω_m than the fiducial value.

Table 11. Fiducial Cosmologies tested in Section. 8 on QPM mocks.

Cosmology	Ω_{CDM}	Ω_M	Ω_B	Ω_Λ	h
AND	0.228286	0.274	0.0457143	0.726	0.7
QPM	0.244143	0.29	0.0458571	0.71	0.7

Table 12. Derived Distances at z=0.57. $\alpha_{\rm exp}$ and $\epsilon_{\rm exp}$ are the expected shifts in the fitted parameters for fact of using the wrong cosmology. The sound horizon is evaluated using CAMB (Lewis et al. 2000)

Cosmo	H(z) km /s/Mpc	$D_A(z)$ Mpc	r_s Mpc	$D_V(z)$ Mpc	$\alpha_{\rm exp}$	$\epsilon_{\rm exp}$
AND	93.6	1359.6	149.28	2027.0	1.0064	-0.0021
QPM	94.7	1351.1	147.21	2009.5	1.0	0.0

where

$$D_V = [cz(1+z)D_A^2(z)/H(z)]^{1/3}. \quad (25)$$

The bias b_α and b_ϵ are defined as follows:

$$b_\alpha = <\alpha> - \alpha_{\rm exp} \quad , \quad (26)$$

$$b_\epsilon = <\epsilon> - \epsilon_{\rm exp}. \quad (27)$$

The expected values for each cosmology are: $\alpha_{\rm exp}^{\rm QPM} = 1.0, \epsilon_{\rm exp}^{\rm QPM} = 0.0, \alpha_{\rm exp}^{\rm And} = 1.0064, \epsilon_{\rm exp}^{\rm And} = -0.0021$. Substituting the cosmological parameters in equations 23 and 25, and evaluating at $z = 0.57$, we get that the expected shifts are $b_\alpha = 0.6\%$ and $b_\epsilon = -0.2\%$ for Anderson Cosmology (AND) (Table 12).

In Table C5 we show the results of fitting 100 mocks for this test, pre and post reconstruction using a different cosmology in the analysis from the natural cosmology of the mocks. The covariance matrix used was generated from 1000 NGC mocks in QPM cosmology. Figure 11 shows the dispersion plots of α, ϵ from performing BAO anisotropic analysis using two different fiducial cosmologies; we observe that best fitting values are well correlated but need to be re-scaled accordingly to the expected shift. The bias observed in the two cosmologies pre-reconstruction are very similar ~ 0.2 %; the bias is reduced post-reconstruction, the mocks in the QPM cosmology show a bias $b_\alpha = -0.0006$. The mocks in the Anderson cosmology shows a bias of 0.0003%. We summarized the differences in the bias observed in Table 13. These differences in bias will serve to estimate the systematic shift associated to the fiducial cosmology. When analyzing the mocks with the "true" cosmology we measure the intrinsic bias coming from: 1) Non linear evolution of the density perturbations and 2) bias of the fitting methodology.

Table 13. Fiducial cosmology related systematics. Fitting results from 100 QPM NGC mocks pre-/post- reconstruction using a different cosmology in the analysis from the natural cosmology of the mocks. The different columns are the mean difference between bias, i.e. $\Delta b_\alpha = b_\alpha^{\rm true} - b_\alpha^{\rm wrong}$, the analogue for ϵ. The covariance matrix used was generated from 1000 NGC mocks in QPM cosmology.

Fiducial Cosmology related Systematics		
DR11 CMASS QPM mocks, Pre/Post-Reconstruction		
Sample	Δb_α	Δb_ϵ
Pre-recon	0.0002	<0.0001
Post-recon	0.0009	0.0010

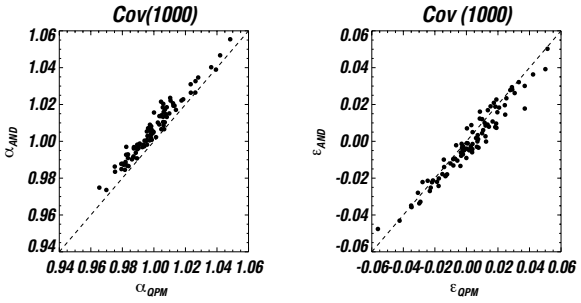

Figure 11. Dispersion plots of α, ϵ from performing BAO anisotropic analysis using two different fiducial cosmologies.

We do expect to reduce the first contribution in post-reconstruction. When considering a "wrong cosmology" any extra contribution to the bias can be associated with the cosmology mismatch. We have a shift of 0.0024 on α for the true cosmology, which becomes to 0.0006 post-reconstruction. The reduction observed is related just to removal of the non linear evolution of the density field. The extra bias of 0.0009 in α and 0.0010 in ϵ ($\Delta b_\alpha, \Delta b_\epsilon$ in Table 13) observed when using Anderson cosmology is related to the "wrong cosmology" assumed.

We conclude that the systematic error in BAO distance measurements associated to fiducial methodology is 0.0009 for α and 0.0010 for ϵ.

9 SYSTEMATICS UNCERTAINTIES RELATED TO ANISOTROPIC FITTING METHODOLOGY

The anisotropic fitting methodology has been extensively tested (Xu et al. 2012a; Anderson et al. 2013, 2014; Vargas-Magana et al. 2014; Ross et al. 2012) and the methodology is well established. However, we can still explore the sub percent uncertainties coming from the fitting methodology. In this section we explore some of them that have not been previously explored, that need to be revisited in the context of the BOSS final analysis.

9.1 Damping Model

Recent developments in the modelling of the damping have been proposed and tested (Seo et al. 2016; Ross et al. 2016; Beutler et al. 2016a; Alam et al. 2016). We test the so-called "Gaussian Damping Model", our fiducial damping model, given by:

$$C_G(k,\mu,z) = (1+\beta\mu^2)\exp\left[-\frac{k^2(1-\mu^2)\Sigma_\perp - k^2\mu^2\Sigma_{||}}{4}\right], \quad (28)$$

against the modified Gaussian model, given by the following equation:

$$C_{MG}(k,\mu,z) = (1+\beta\mu^2(1-S(k))\exp\left[-\frac{k^2(1-\mu^2)\Sigma_\perp - k^2\mu^2\Sigma_{||}}{4}\right]. \quad (29)$$

This modified Gaussian damping model suits better the reconstruction algorithm applied in this paper Seo et al. (2016). The Gaussian model was used in DR12 CMASS/LOWZ analysis (Cuesta et al. 2016; Vargas-Magana et al. 2015; Gil-Marín et al. 2016) and the Modified Gaussian model is used in the final BOSS analysis (Ross et al. 2016; Beutler et al. 2016a; Alam et al. 2016). In Figure 12 we show the dispersion plots of the best fits using both variants of the damping model applied to the lower redshift bin. The best fits are not affected by this variant of the model; there is just a small dispersion on ϵ.

Table 14. Fitting Systematic Error: Damping Model. We summarize the variations $\Delta\alpha$, $\Delta\epsilon$ observed from the different combinations from Table C7.

DR12 Pre-Reconstruction						
Model	b_α	b_ϵ	$\Delta\alpha$	$\Delta\epsilon$	$\Delta\sigma_\alpha$	$\Delta\sigma_\epsilon$
Bin 1 ($0.2 < z < 0.5$)						
C_G	-0.0007	0.0007	-	-	-	-
C_{MG}	-0.0007	0.0011	<0.0001	0.0004	0.0003	0.0019
Bin 1 ($0.2 < z < 0.5$)						
C_G	0.0010	0.0021	-	-	-	-
C_{MG}	0.0010	0.0023	<0.0001	0.0005	0.0004	0.0022
Bin 1 ($0.2 < z < 0.5$)						
C_G	0.0008	0.0009	-	-	-	-
C_{MG}	0.0007	0.0008	0.0001	0.0010	0.0002	0.0019

Table C7 shows the results of fitting using these two versions of the damping model in the Combined Sample for the three redshift bins. For determining the systematical error we compute as before the variation in the mean values. We get $\Delta\alpha = [< 0.0001, < 0.0001, 0.0001]$ and $\Delta\epsilon = [0.0004, 0.0005, 0.0010]$ for the three redshift bins, taking the RMS of the three cases we get $\Delta\alpha < 0.0001$, $\Delta\epsilon = 0.0007$.

In addition to the determining the variation in the mean values , we would like to check the effects on the error distributions. In the case of the Gaussian damping the results indicate that the variation of the damping model affects ϵ uncertainties. Figure 13 shows the error distributions in both cases: Gaussian and Modified Gaussian damping. The Modified Gaussian model is giving smaller errors compared to the Gaussian model. According to Table C7, the differences in the error distributions are $\Delta\sigma_\alpha = [0.0003, 0.0004, 0.0002]$ and $\Delta\sigma_\epsilon = [0.0019, 0.0022, 0.0019]$, taking the RMS we get $\Delta\sigma_\alpha = 0.0003$ and $\Delta\sigma_\epsilon = 0.0020$.

We conclude that the systematic error in BAO distance measurements associated to Damping Model is $\Delta\alpha < 0.0001$, $\Delta\epsilon =$

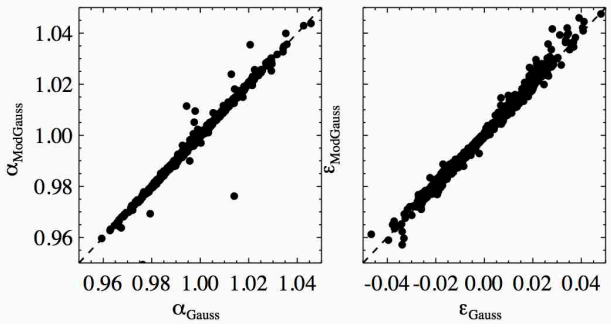

Figure 12. Dispersion plots of α and ϵ from MD-PATCHY for 1000 mocks lower bin Post-reconstruction using two variants of the model for the Damping: Gaussian and Modified Gaussian .

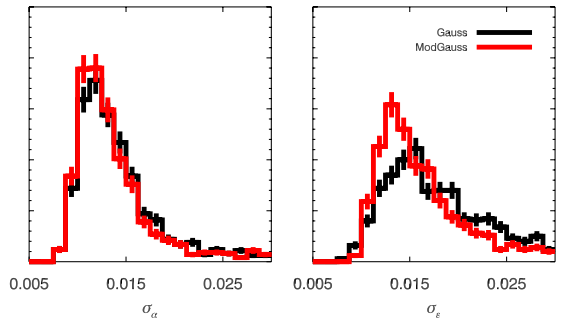

Figure 13. Error distributions from MD-PATCHY for 1000 mocks lower redshift bin Post-reconstruction using two variants of the model for the Damping: Gaussian and Modified Gaussian.

0.0007. The variations in the error distributions are $\Delta\sigma_\alpha = 0.0003$ and $\Delta\sigma_\epsilon = 0.0020$.

9.2 Hexadecapole contribution

Usually the hexadecapole is not used on BAO fits because of its small signal to noise ratio. Furthermore, after reconstruction its amplitude is reduced even more, decreasing its importance. We compare in this subsection, our fiducial methodology considering only monopole+ quadrupole against the fits using monopole+quadrupole+hexadecapole. In Figure 1 top panels we show the mean monopole, quadrupole and hexadecapole from 1000 PATCHY Combined mocks pre- and post-reconstruction for the three redshift bins. The figure demonstrates that, before reconstruction, the hexadecapole is significantly smaller compared with the monopole and quadrupole. Post-reconstruction reduces even more the hexadecapole contribution. Also the mean hexadecapole of 1000 mocks is significantly noisier compared to the means of the multipoles $\ell = 0, 2$.

We perform anisotropic BAO fits following the methodology described in Section 2 but this time we consider also the hexadecapole and compare it with the fits using only the monopole+quadrupole (denoted by $l = 0, 2$ hereafter). The sample covariance used on the fits is shown in top panels of Figure D1 for the multipoles estimator. The correlation reveals that, post-reconstruction results in a more diagonal hexadecapole contribution, and the covariance is reduced for the off-diagonal terms.

In Table 15 we show the results of performing the BAO

Table 15. Fitting Systematic Error: Hexadecapole. We summarize the variations $\Delta\alpha$, $\Delta\epsilon$ observed from the different combinations from Table C8.

DR12 Pre-Reconstruction						
Max. Mulipole	b_α	b_ϵ	$\Delta\alpha$	$\Delta\epsilon$	$\Delta\sigma_\alpha$	$\Delta\sigma_\epsilon$
Bin 1 ($0.2 < z < 0.5$)						
$\xi_{l=2}$	-0.0007	0.0007	-	-	-	-
$\xi_{l=4}$	-0.0009	0.0004	0.0002	0.0003	0.0016	0.0034
Bin 1 ($0.2 < z < 0.5$)						
$\xi_{l=2}$	0.0010	0.0021	-	-	-	-
$\xi_{l=4}$	0.0007	0.0018	0.0003	0.0003	0.0014	0.0030
Bin 1 ($0.2 < z < 0.5$)						
$\xi_{l=2}$	0.0008	0.0009	-	-	-	-
$\xi_{l=4}$	0.0008	0.0009	<0.0001	<0.0001	0.0014	0.0030

anisotropic analysis to the 1000 PATCHY mocks, pre and post-reconstruction. The best fit results indicate that differences of using $\ell = 0, 2$ compared with $\ell = 0, 2, 4$ are not significant. In the $\alpha - \epsilon$ fits; the variation in the mean vales are, taking the RMS of the three cases, $\Delta\alpha$, $\Delta\epsilon$=0.0002 post-reconstruction. The small effect on the best fitting values confirms previous results from Ross et al. (2015) that demonstrate the monopole and quadrupole represent a complete and optimal set of estimators in the case where information is spherically distributed.

In addition to quantify systematic errors we also test the effect on the uncertainties. Figure 15 shows the error distributions of the post-reconstruction fits in the three redshift bins. The figure illustrates for the lower redshift bin that including hexadecapole information (i.e., monopole+quadrupole+hexadecapole), the error distributions show differences with respect to the only monopole-quadrupole fits.Results indicate that using the hexadecapole reduces the mean uncertainties by, taking the RMS , $\Delta\sigma_\alpha = 0.0015$ and $\Delta\sigma_\epsilon = 0.0032$.

Beutler et al. (2016b) (companion paper), analyses the same mocks in Fourier Space comparing also the fits monopole+quadrupole+hexadecapole with the monopole+ quadrupole case for performing RSD analysis. Their results indicate the dispersion is decreased when considering the hexadecapole, in our results, the reduction in the dispersion is smaller in the best fit values.

We conclude that the systematic error in BAO distance measurements associated to using monopole+ quadrupole against the fits using monopole+quadrupole+hexadecapole is 0.0002 for α and ϵ. The variations in the mean error distributions are $\Delta\sigma_\alpha = 0.0015$ and $\Delta\sigma_\epsilon = 0.0032$.

9.3 Fitting range

We revisit the impact of the fitting range on the anisotropic BAO results. The fitting range depends on the template and the noise. Increasing the maximum scale included in the fitting implies a trade-off between increasing the number of bins, and increasing the noise contribution to the fit. On the other hand, the minimum scale is related directly to the accuracy of the template and its capability to

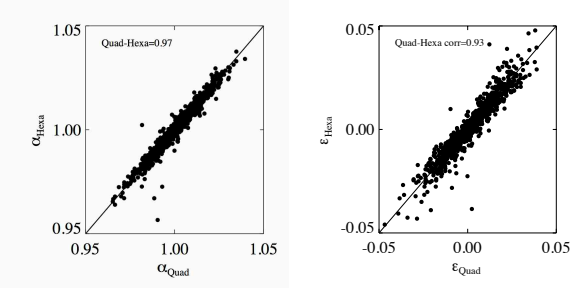

Figure 14. Dispersion plots comparing multiples $\ell = 2$ compared with $\ell = 4$ for 1000 MD-PATCHY post-reconstruction for the lower redshift bin.

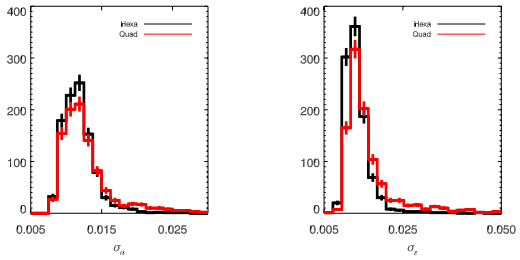

Figure 15. Error Distribution for 1000 MD-PATCHY post-reconstruction for the intermediate redshift bin.

fit the small scales accurately, or that the broadband terms can absorb the mismatch between the template and the measurements. We examine the results in terms of the $\chi^2/d.o.f$ values. Our fiducial choice is a range of (60,155 h^{-1}Mpc), using 5 h^{-1}Mpc bins results in 20 bins.

Table 16 shows the results of fitting 1000 PATCHY mocks for the intermediate redshift bin. The results show that the fits are robust against fitting range variations except when the lower bound is close to the BAO scale, (70-80 h^{-1}Mpc) or going to very small scales (30 h^{-1}Mpc), which gives significantly biased results. In the case of the upper bounds, the results indicate that the fits are very stable against variations of the upper bound of the fits for the values not too close to the BAO (i.e larger 130 h^{-1}Mpc). For our error budget account we consider the results that are shows the smaller bias (i.e only lower bounds of 40-60 and upper bounds larger than 140) we found the variations in $\Delta\alpha, \Delta\epsilon$ quoting the RMS of the different cases : $\Delta\alpha = 0.0002$ and $\Delta\epsilon = 0.0002$.

Concerning the variations in the mean error of the distributions they are small (again only considering the cases that shows small biases i.e only lower bounds of 40-60 h^{-1}Mpc and upper bounds larger than 140 h^{-1}Mpc) we find and RMS variation of $\Delta\sigma_\alpha = 0.0011$ and $\Delta\sigma_\epsilon = 0.0018$. The performance of the fits depends on the details in the modelling and anisotropic methodology. A better model allow us to include smaller scales in the fitting. Using large scales can provide more information but also increases the noise. In Ross et al. (2016) (companion paper); the fitting range is also tested. They found an optimal range of 60-160 h^{-1}Mpc, which is the fiducial range we use in this paper. However, according to our results, in our methodology increasing the upper bound to 180 h^{-1}Mpc will decrease the error by 0.0011 (8%) in α and 0.0019 (12%) in ϵ.

We conclude that the systematic error in BAO distance measurements associated to range of the fits considering only non biased results (i.e lower limit between 40-60 h^{-1}Mpc and upper limit larger than 140 h^{-1}Mpc) is 0.0002 for α and 0.0002 for ϵ. The variations in the error distributions could be as large as 0.0011 in σ_α and 0.0019 in σ_ϵ.

Table 16. Fitting Systematic Error: Range. We summarize the variations $\Delta\alpha$, $\Delta\epsilon$ observed from the different combinations from TableC9. First block refers to variations of the minimum scale fixing the upper limit to 160 h^{-1}Mpc. Second Block, refers to variations of the maximum scale fixing the lower limit to 55 h^{-1}Mpc.

DR12 Pre-Reconstruction						
Min range	b_α	b_ϵ	$\Delta\alpha$	$\Delta\epsilon$	$\Delta\sigma_\alpha$	$\Delta\sigma_\epsilon$
Bin 1 ($0.2 < z < 0.5$)						
30	0.0041	0.0034	0.0031	0.0013	0.0031	0.0013
40	0.0011	0.0023	0.0001	0.0002	0.0002	0.0006
50	0.0010	0.0021	0.0001	0.0002	0.0003	0.0005
60	0.0011	0.0023	-	-	-	-
70	−0.0007	0.0010	-0.0017	-0.0011	-0.0004	-0.0020
80	0.0208	0.0248	0.0195	0.0229	0.0061	0.0174
Max range	b_α	b_ϵ	$\Delta\alpha$	$\Delta\epsilon$	$\Delta\sigma_\alpha$	$\Delta\sigma_\epsilon$
120	0.0017	0.0010	0.0007	-0.0011	0.0033	0.0053
130	−0.0001	0.0011	-0.0011	-0.0010	0.0023	0.0039
140	0.0005	0.0017	0.0004	-0.0002	-0.0013	-0.0024
155	0.0010	0.0021	-	-	-	-
160	0.0009	0.0019	-0.0001	-0.0002	-0.0001	-0.0003
170	0.0011	0.0020	-0.0002	0.0001	0.0010	0.0016
180	0.0011	0.0021	-0.0002	0.0002	0.0011	0.0019

9.4 Bin centres

We vary the bin centre, maintaining the bin width to test whether this change affects the anisotropic fitting results. Fixing the bin size to 5 h^{-1}Mpc we shifted the bin centre by 1, 2 ,3, and 4 h^{-1}Mpc compared with the fiducial choice that is 0 h^{-1}Mpc shift. [9]

Table 14 shows the fitting results with the different bin centres shifted compared with the fiducial choice. The bias of all measurements is similar for all cases (< 0.0006). We measure variations on the mean values of α and ϵ taking the RMS of the different cases: $\Delta\alpha = 0.0002$ and $\Delta\epsilon = 0.0004$. We conclude that the systematic error in BAO distance measurements associated to bin centres is 0.0002 for α and 0.0004 for ϵ for the three redshift bins.

10 APPLICATION TO BOSS DATA

We now apply our methodology as described in Sec. 2 to our BOSS dataset. We test if the offsets between measured data parameters

[9] This test also allows us to better compare the power spectrum with the configuration space fits. This is because we expect that the average of the measurements performed over different centre bins will be strongly correlated with the power spectrum measurements.

Table 17. Fitting Systematic Error: Bin Centre. We summarize the variations $\Delta\alpha$, $\Delta\epsilon$ observed from the different combinations from Table C7.

DR12 Pre-Reconstruction				
Bin Centre	b_α	b_ϵ	$\Delta\alpha$	$\Delta\epsilon$
Bin 1 ($0.2 < z < 0.5$)				
0 h^{-1}Mpc	0.0008	0.0021	-	-
1 h^{-1}Mpc	0.0010	0.0021	0.0002	<0.0001
2 h^{-1}Mpc	0.0010	0.0017	<0.0001	0.0004
3 h^{-1}Mpc	0.0007	0.0015	0.0003	0.0006
4 h^{-1}Mpc	0.0009	0.0018	0.0001	0.0003

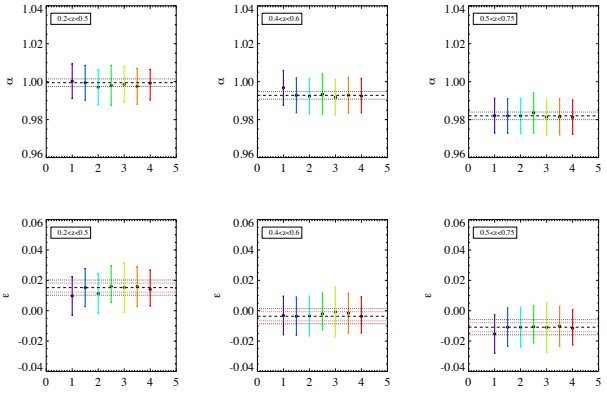

Figure 18. Fits and errors from fitting the low redshift bin of BOSS data. (Top) α and σ_α from fitting using a variation in the BAO methodology. (Bottom) ϵ and σ_ϵ, the dashed lines are the fiducial case of the different measurements, the dotted line in α plots correspond to a difference from the mean of 0.2%, the dotted lines in ϵ plots are in 0.3%(red) and 0.5% respectively.

from variants of the methodology and the fiducial best-fit values, are consistent with those from the mocks. We use the final BOSS combined catalogue from SDSS-DR12, as described in Sec. 2.1. We apply all weights that are described in Ross et al. (2016) which included weights related to seeing, stellar densities, fibre collisions, redshift failures and the FKP weights to reduce the variance in clustering measurements. We first calculate the pair-counts from the catalogues, and then compute the various clustering estimators before reconstruction as seen in the left panels of Figure 16 top panels for multipoles, intermediate panels for Wedges and bottom panels for ω_l clustering estimator. The data points are the error bars, and the solid lines are the mean from the mocks. We then apply our reconstruction algorithms to our data, and show the resulting clustering estimators for the data in the right panels of Figure 16 for all three redshift bins in the catalogue. The error bars are given by the diagonal terms of the covariance matrix computed from the 1000 MD-PATCHY mock catalogues. We notice the data measurements: monopole, quadrupole and hexadecapole are consistent with the behaviour observed on the mocks. The new feature in this plot is the hexadecapole contribution which is very small even pre-reconstruction and noisy. The hexadecapole contribution post-reconstruction presents a reduction of the amplitude and of the associated error bars. The clustering wedges ($\xi_{||,\perp}$) and the ω data measurements are also consistent with the behaviour observed on the mocks.

The results of applying the anisotropic fitting methodology to the COMBINED samples of BOSS are presented in Table 18 for the three redshift bins, considering the different variations of the methodology explored in the paper. One aspect to notice is that at least for the DR12 data, the uncertainty found from the ω-estimator is almost the same as for the standard multipoles (some bins are a little better, some are a little worse), so you can say that it would make very little difference which one we choose for the consensus result, but we might expect the ω-estimator to perform the best in the future.

We analyze the differences in the values of α and ϵ generated for the variations of the methodology ($\Delta\alpha$ and $\Delta\epsilon$) in Table 18, and their consistency with the mocks results. We start analyzing the lower redshift bin. The results are shown in Figure 17, we show how the $[\Delta\alpha^{\rm DR12}, \Delta\epsilon^{\rm DR12}]$ observed in DR12 compares with the $\Delta\alpha^{\rm MOCKS}$, $\Delta\epsilon^{\rm MOCKS}$ observed in the mocks for the three redshift bins. From the figures we conclude the variations observed on the data are completely consistent with the results obtained with the mocks for the lower redshift bin, as most of them lie within 1-σ contour. Only the hexadecapole case lies outside the $1-\sigma$ contours for the lower redshift bin.

Figure 18 shows the best fits obtained from applying the variants of the methodology study in the paper to DR12 final data samples. The first row of plots shows results for α best fits values for the three redshift bins. The dashed line indicates the measurement for the fiducial methodology and the dotted lines are the 0.2% variations with respect to the fiducial case. As we can observe, the different measurements from all three redshift bins lie within $\Delta\alpha = \pm 0.002$ except one measurement in the intermediate redshift bin for the hexadecapole. The bottom plots are for ϵ measurements; the same colour coding is used, but in this case we included two dotted lines, the first red dotted line indicates the $\Delta\epsilon = \pm 0.003$, the second $\Delta\epsilon = \pm 0.005$. For ϵ the results indicate that, for the intermediate and high redshift bins, almost all measurements are within the first dotted lines. The lower redshift bin shows slightly more dispersion of the measurements, but all of them are within $\Delta\epsilon = \pm 0.005$.

11 SYSTEMATIC ERROR BUDGET

The aim of this paper is to provide final numbers for the distance measurements $D_V(z)$, $D_A(z)$, $H(z)$ for the three redshift bins which include the systematic error coming from the theoretical systematics explored in this paper. In previous sections, we have tested several variations of the fiducial methodology. We conclude that all of them give statistically unbiased measurements with comparable error bars so there is no strong reason to prefer one method over the rest. In previous sections we picked a fiducial pipeline, and we tested how variations of this pipeline change the results using the mock catalogues measuring the difference in the mean values of the best fit parameters between fiducial and the variant, this provides us the contribution to the error budget for a particular variant of the methodology. Every change was made one-at-a-time, i.e in this first estimate of the error budget, we are neglecting possible correlations between effects.

In Tables 19, 20, 21 we summarize our findings for pre-reconstruction, post-reconstruction results. For these three tables we quote the $\Delta\alpha$ and $\Delta\epsilon$ (eq.22) over every method variation computed using the main table of the corresponding section (RMS of differences between the means obtained of each kind of variations and the fiducial case). The numbers post-reconstruction are also

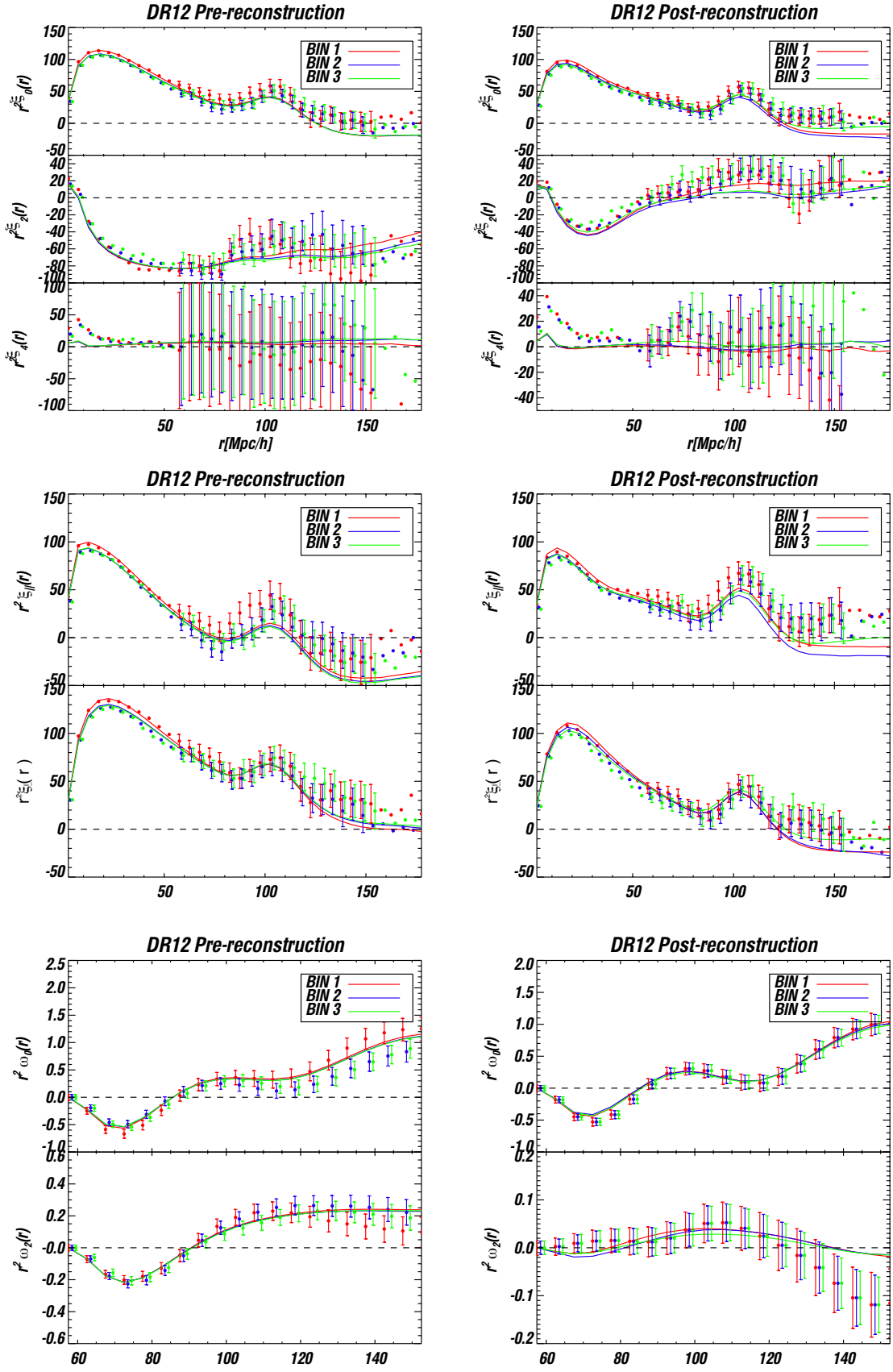

Figure 16. Top panels: Multipoles of the final BOSS combined sample pre-reconstruction (left panel) and post-reconstruction (right panel) in three redshift bins. Intermediate panels: Same as before for clustering wedges. Bottom panels: ω_l clustering statistics. Error bars represent the data, and solid line represent the mean of the mocks.

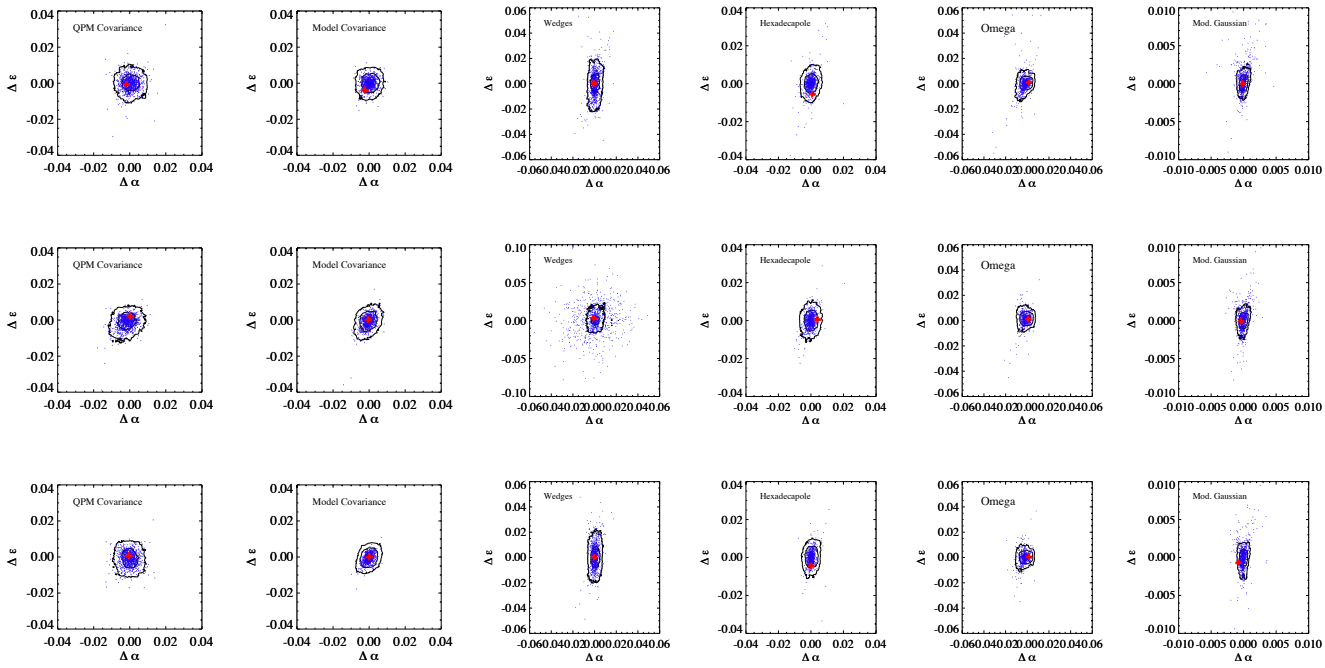

Figure 17. We show how the $[\Delta\alpha^{\rm DR12}, \Delta\epsilon^{\rm DR12}]$ observed in DR12 [red cross] compares with the $\Delta\alpha^{\rm MOCKS}$, $\Delta\epsilon^{\rm MOCKS}$ observed in the mocks [black dots] for the following six variants of the methodology (from left to right, and top to bottom): QPM covariance, model covariance, wedges estimator, hexadecapole contribution, ω_ℓ-estimator and modified Gaussian damping model, respectively. The top panels corresponds to the lower redshift bin and the centre and bottom panels for the intermediate and higher redshift bins respectively.

quoted in the concluding statement in the respective section. We consider only the cases that produce unbiased measurements, i.e we eliminate the cases where the modification is significantly biasing the measurements (ex. extending the lower bound of the fits produce a bias of 0.3%).

We start briefly discussing pre-reconstruction results. These results are presented in Tables 19. We present two blocks: first block devoted to the results obtained from this work and a second block including previous results on theoretical systematics uncertainties in BAO analysis. The results indicate that the main contribution for the error comes from the estimators choice which shows large variations in the best fits of $\Delta\alpha = 0.004$ and $\epsilon = 0.006$). From the second block, the larger contribution is coming from the template in the case of α (0.006), all other contributions are contributing less than 0.001. The total error budget pre-reconstruction adding in quadrature all the terms is 0.007 in α and ϵ.

Post-reconstruction results are split into Tables (20 and 21), the first of which summarizes the error budget for Alam et al. (2016) and the second of which shows the results of the tests that, do not contribute for the error budget, but still provides insights about variations in the best fits parameters. The first block in Table20, presents the results on combined sample from this work. We include separately the cosmology test (in a second block) as this test was performed with fewer mocks and with different sample (CMASS). The third block include results from Alam et al. (2016) related to the estimator, the variations on the estimator relates to the consensus values[10] compared to the results in configuration space from this work. We also include a fourth block including the findings of previous researches on theoretical systematics uncertainties in BAO analysis. Vargas-Magana et al. (2014) analysed the potential systematics in BAO fitting methodology using mocks and data from BOSS DR10 and DR11 for CMASS sample.The methodological changes tested are: (i) Model Templates ; (ii) Fitting Range and Bin Sizes; (iii) Nuisance Terms Model; iv) Priors; v) Non linear damping parameters $\Sigma_{||,\perp}$ and Streaming model Σ_s . The variations in α and ϵ observed in the first block are all below 0.0017 for α and 0.0019 for ϵ. The variations in α and ϵ observed post-reconstruction are in all cases $\Delta\alpha, \Delta\epsilon < 0.001$. The dominant term in α error comes from the covariances (first block), fiducial cosmology (both of contributing similarly) and the reconstruction step that is the largest error contribution to the systematic error budget. If we just consider the smoothing scale of 10 h^{-1}Mpc an not smaller smoothing scales this contribution decrease to similar level as the covariance and the fiducial tests. For ϵ, the dominant terms are the estimator, covariance, fiducial cosmology, broad band terms and non linear damping, all of them contributing in a similar fraction, followed by the damping model.

Our estimate of the error budget is obtained adding in quadrature all the sources of systematic errors. One caveat on this estimate are the tests performed with an small number of mocks, while testing with $\sim$100 mocks is enough for determine if a methodology is biased, for getting the bias to the precision required for our measurements we need more mocks. Even though, we decided to consider the bias obtained from the test with few mocks in the error budget. Further work should be done to determine with more precision these biases in future surveys as (eBOSS, DESI). The numbers in parenthesis for ϵ indicates the total when, instead of using our accounting of the systematic error related to the estimators, we use the systematic error coming from comparing our fiducial

[10] The consensus values result from combining optimally Fourier space multipoles (Beutler et al. 2016a) and configuration space multipoles.

Table 18. Fitting results from Combined DR12 samples in the low redshift bin. Δx is the difference with respect to the fiducial case (first row)

Testing Variants of Methodology on DR12							
DR12 Combined Samples Post-reconstruction							
BIN 1 ($0.2 < z < 0.5$)							
Variable	$\alpha \pm \sigma_\alpha$	$\Delta\alpha$	$\Delta\sigma_\alpha$	$\epsilon \pm \sigma_\epsilon$	$\Delta\epsilon$	$\Delta\sigma_\epsilon$	χ^2
PAT cov	0.9995 ± 0.0098	-	-	0.0152 ± 0.0125			1.41
QPM cov	0.9976 ± 0.0091	-0.0019	-0.0007	0.0159 ± 0.0119	0.0007	-0.0006	1.47
Model Cov	0.9971 ± 0.0090	-0.0023	-0.0008	0.0113 ± 0.0118	-0.0039	-0.0006	1.37
$\xi_{\parallel,\perp}$	0.9986 ± 0.0103	-0.0009	0.0005	0.0153 ± 0.0154	0.0001	0.0029	1.16
$\xi_{l=4}$	1.0002 ± 0.0097	0.0008	-0.0001	0.0097 ± 0.0102	-0.0055	-0.0022	1.32
ω_l	0.9980 ± 0.0094	0.0015	-0.0004	0.0160 ± 0.0132	0.0008	-0.0007	1.41
$C_{MG,60}$	0.9993 ± 0.0099	-0.0002	0.0000	0.0140 ± 0.0127	-0.0012	0.0002	1.36
BIN 2 ($0.4 < z < 0.6$)							
Variable	$\alpha \pm \sigma_\alpha$	$\Delta\alpha$	$\Delta\sigma_\alpha$	$\epsilon \pm \sigma_\epsilon$	$\Delta\epsilon$	$\Delta\sigma_\epsilon$	χ^2
PAT	0.9928 ± 0.0084	-	-	-0.0036 ± 0.0107	-	-	0.63
QPM cov	0.9929 ± 0.0080	0.0001	-0.0004	-0.0016 ± 0.0103	0.0021	-0.0004	0.69
Model cov	0.9923 ± 0.0078	-0.0005	-0.0006	-0.0035 ± 0.0106	0.0002	-0.0001	0.68
$\xi_{\parallel\perp}$	0.9917 ± 0.0089	-0.0010	0.0005	-0.0008 ± 0.0140	0.0029	0.0034	0.66
$\xi_{l=4}$	0.9968 ± 0.0088	0.0040	0.0004	-0.0032 ± 0.0099	0.0005	-0.0008	2.22
ω_l	0.9935 ± 0.0087	0.0007	0.0003	-0.0020 ± 0.0102	0.0011	-0.0005	0.70
C_{MG60}	0.9924 ± 0.0083	-0.0004	-0.0001	-0.0037 ± 0.0100	-0.0001	-0.0007	0.62
BIN 3 ($0.5 < z < 0.75$)							
Variable	$\alpha \pm \sigma_\alpha$	$\Delta\alpha$	$\Delta\sigma_\alpha$	$\epsilon \pm \sigma_\epsilon$	$\Delta\epsilon$	$\Delta\sigma_\epsilon$	$\chi^2/d.o.f$
PAT cov	0.9820 ± 0.0091	-	-	-0.0109 ± 0.0125	-	-	0.97
QPM cov	0.9815 ± 0.0094	-0.0005	0.0003	-0.0102 ± 0.0131	0.0006	0.0006	1.04
Model cov	0.9820 ± 0.0092	0.0000	0.0001	-0.0109 ± 0.0130	0.0000	0.0005	0.97
$\xi_{\parallel\perp}$	0.9813 ± 0.0094	-0.0004	0.0003	-0.0110 ± 0.0163	0.0001	0.0038	1.08
$\xi_{l=4}$	0.9821 ± 0.0091	0.0001	0.0000	-0.0153 ± 0.0127	-0.0044	0.0001	1.59
ω_l	0.9836 ± 0.0094	0.0016	0.0010	-0.0105 ± 0.0116	0.0004	0.0009	1.23
C_{MG60}	0.9812 ± 0.0088	-0.0008	-0.0003	-0.0116 ± 0.0108	-0.0007	-0.0017	1.00

results with the consensus values. The main difference is that that systematic error in α decreases to be negligible, in the other side, the systematic error in ϵ increases and becomes the most important contribution to the error budget. The difference in ϵ values in this case is driven by the differences between FS and CS estimators.

Combining all sources of theoretical systematic uncertainty, we find $\Delta\alpha \approx 0.002$ and $\Delta\epsilon \approx 0.003$ for all three redshift bins (see the "Total 1+ Total 2" row in Table 21 for more precise figures). Simply combining these results in quadrature implicitly assumes that each source of uncertainty is independent, and so we regard these estimates as upper bounds rather than the best possible estimates. Crucially, we find that non-reconstruction related sources of theoretical systematic uncertainty (everything in Table 20 except second block) in α all combine to make a contribution that is dominated by the uncertainty related to reconstruction techniques (second block in Table 20).

12 FINAL DISTANCE CONSTRAINTS FROM DR12.

In this section we present our final BAO measurements for the combined galaxy samples from BOSS DR12 in the three redshift bins. We translate our measurements on α and ϵ estimated with our fiducial cosmology into distance measurements following equations 10, 11, and 12. We include the systematic error in α and ϵ as estimated in previous section. We quote in Table 22 our final distance constraints from the analysis of the BAO in the correlation function of BOSS combined sample. We quote our results in the angle-averaged distance $D_V(z)$, the Hubble parameter $H(z)$, and the angular diameter $D_A(z)$. We quote the two contributions to the error as $(\sigma_{\rm stat}, \sigma_{\rm sys})$, so that the total error is the sum in quadrature of both quantities ($\sigma^2_{\rm tot} = \sigma^2_{\rm stat} + \sigma^2_{\rm sys}$).

The final constraints on the angular diameter distance $D_A(z)$ and the Hubble parameter $H(z)$ including both statistical and the-

Table 19. Summary of Theoretical Systematic Errors Pre-reconstruction. We quote the maximal $\Delta\alpha$ and $\Delta\epsilon$ (eq.22) over every method variation computed using the main table of the corresponding section (maximal difference between the means obtained of each kind of variations and the fiducial case).The first block corresponds to the findings in this work. The case of Fiducial Cosmology is treated separately as it was performed with an small number of simulations and with sample CMASS. The third block corresponds to the findings of previous works. We also include a total.

DR12 Pre-Reconstruction				
Mocks	Sample	Source of Uncertainty	$\Delta\alpha$	$\Delta\epsilon$
PATCHY(1000)	COMBINED	Estimator (Section 4)	0.0047	0.0057
QPM(1000)	COMBINED	Randoms (Section 5)	0.0008	0.0006
QPM/PATCHY(1000)	COMBINED	Covariance (Section 6)	0.0008	0.0030
*PATCHY(1000)	COMBINED	Hexadecapole (Section 9)	0.0002	0.0003
QPM(100)	CMASS	Fiducial Cosmology (Section 8)	0.0002	< 0.0001
PTHALOS(600)	CMASS	Fitting Templates (Vargas-Magana et al. 2014)	0.0055	0.0004
PTHALOS(600)	CMASS	Fitting Bin Size (Vargas-Magana et al. 2014)	0.0003	0.0002
PTHALOS(600)	CMASS	Fitting Priors (Vargas-Magana et al. 2014)	0.0002	0.0006
PTHALOS(600)	CMASS	Fitting Nuisance T. (Vargas-Magana et al. 2014)	0.0005	0.0006
PTHALOS(600)	CMASS	Fitting Streaming (Vargas-Magana et al. 2014)	0.0003	0.0007
PTHALOS(600)	CMASS	Fitting NL damping (Vargas-Magana et al. 2014)	0.0005	0.0033
Total			0.0071	0.0074

oretical systematic uncertainty are 1.5% and 2.8% for the low redshift bin ($z_{\rm eff} = 0.38$), 1.4% and 2.4% for the intermediate redshift bin ($z_{\rm eff} = 0.51$) and 1.7% and 2.6% for the high redshift bin ($z_{\rm eff} = 0.61$). The constraints on $D_V(z)$ are 1.0%, 0.9%, and 1.0% for these three redshift bins.

In Figure 19 we present the constraints 1-2σ for $D_A(z)$ and $H(z)$ for the three samples at $z_{\rm eff} = 0.38, 0.51, 0.61$ from the fiducial methodology: analysis of correlation function multipoles using the covariance matrix from MD-PATCHY mock catalogues. We include the contours without the contribution of the systematic errors in dashed lines just as a reference. We also included the constraints from Planck 2015 (Planck Collaboration et al. 2015b) temperature and polarisation power spectrum data assuming a ΛCDM model. BOSS results are in agreement with Planck results as shown in the figure. The cosmological implications are presented in the BOSS collaboration paper (Alam et al. 2016, companion paper), where the different measurements are cross-checked and combined.

13 CONCLUSIONS

In this paper we have presented a detailed investigation of possible sources of theoretical systematics in anisotropic BAO measurements in configuration space. We examined the various steps of the analysis and studied the potential systematics associated with each step presented in the same order as in the analysis. We have applied variations of the methodology to mock catalogues. We can summarize our findings as follows:

• **Estimators.** We analyzed different estimators in configuration space: multipoles, wedges, and ω_ℓ estimators . We studied the systematic uncertainties derived from this step in the clustering analysis post-reconstruction. We found differences $\Delta_\alpha = 0.0012$, $\Delta_\epsilon = 0.006$ between different estimators for the three redshift bins. This systematic error could be reduced when combining optimally different estimators as demonstrated in Sánchez et al. (2016b). Concerning the uncertainties, we found differences in the mean uncertainty between $\Delta\sigma_\alpha = 0.0013$ and $\Delta\sigma_\epsilon = 0.0029$ for the post-reconstruction mocks in the three redshift bins.

• **Randoms.** We tested the effect of using different sizes of the random catalogue in anisotropic fits. For the pre-reconstruction case, we tested two cases: $20\times$ and $50\times$. The main conclusion is that the randoms make very small differences in the isotropic/anisotropic fits. The differences observed are < 0.0003 for CMASS mocks. For the post-reconstruction case, we chose a different approach. We reduced the number of randoms from $50\times$ to $4\times$ for post-reconstruction correlation functions in the numerator SS (not for the DS term) and tested the impact in the correlation function and fitting parameters. We found that differences between the $50\times$ and the $4\times$ anisotropic fits are very small ~ 0.0002 for α and ϵ for Combined mocks for all three bins.

• **Covariances.** We explored the effect of using different kinds of mocks to estimate the sample covariance matrix. Also, we tested the new proposed approach of modelling the covariance using O'Connell et al. (2015) methodology calibrated with DR12 combined sample catalogues. We documented the differences we found in the structure of the different covariances; also we showed the results of performing the BAO anisotropic fittings to the mocks using the different covariances. We found differences $\leqslant 0.0009$ for α and $\leqslant 0.0009$ for ϵ for the three redshift bins. The uncertainties distributions are also very similar, we found differences in the mean values $\Delta\sigma_\alpha = 0.0005$ and $\Delta\sigma_\epsilon = 0.0010$.

• **Reconstruction.** We revisited the effect of the smoothing scale on Combined MD-PATCHY mocks. We tested three smoothing scales 5,10,15 h^{-1}Mpc with 100 mocks. We found variations in the best fit parameter in BAO distance measurements associated to the smoothing scale used in reconstruction of the density field 0.0017 for α and 0.0006 for ϵ if we consider smoothing scales of 5 and 10 h^{-1}Mpc. If we only consider differences between 15 and 10 h^{-1}Mpc the variations are only 0.0009 on α and 0.0002 on ϵ.

• **Fiducial Cosmology.** We studied the fiducial cosmology dependence of BAO anisotropic analyses. We analyzed mocks assuming a different fiducial cosmology from the one used to generate the mocks and we compared with results obtained assuming their "true cosmology". We tested flat cosmologies that are shifted in Ω_m by 0.5% compared to true cosmology, but used exactly the same

Table 20. Summary of Theoretical Systematic Errors Post-reconstruction. We quote the $\Delta\alpha$ and $\Delta\epsilon$ (eq.22) over every method variation considered for (Alam et al. 2016) BAO-only error budget. We computed using the main table of the corresponding section (RMS of the differences between the means obtained of each kind of variations and the fiducial case).The first block corresponds to the findings in this work. The cases of Reconstruction/Fiducial Cosmology are presented separately as they were performed with an small number of simulations. We also include in the table as a reference the result from comparing our fiducial methodology to the consensus values from Alam et al. (2016). We consider this number to the final account of the systematic error budget instead of the estimators Multp-Wed, as the consensus value includes the Fourier Space estimator contribution and also the optimal combination method following Sanchez et al 2016. The second block includes the results from previous works on the systematics related to the modelling. We present partial sums of the items as well as a global sum that corresponds to the final error budget for the Alam et al. (2016).

DR12 Post-Reconstruction				
Mocks	Sample	Source of Uncertainty	$\Delta\alpha$	$\Delta\epsilon$
QPM/PATCHY(1000)	COMBINED	Covariance (Section 6)	0.0009	0.0009
PATCHY(1000)	COMBINED	Fitting:Damping (Section 9)	<0.0001	0.0007
PATCHY(1000)	COMBINED	Fitting:Range (Section 9)	0.0002	0.0002
PATCHY(1000)	COMBINED	Fitting:Bin Centre (Section 9)	0.0002	0.0004
PATCHY(100)	COMBINED	Reconstruction Smoothing Scale (Section 7)	0.0017	0.0006
QPM(100)	CMASS	Fiducial Cosmology (Section 8)	0.0009	0.0010
PATCHY(1000)	COMBINED	Estimator Consensus-Fid (Alam et al. 2016)	0.0004	0.0012
Total 1			0.0022	0.0021
Mocks	Sample	Source of Uncertainty	$\Delta\alpha$	$\Delta\epsilon$
PTHALOS(600)	CMASS	Fitting Templates (Vargas-Magana et al. 2014)	0.0003	0.0003
PTHALOS(600)	CMASS	Fitting Bin Size (Vargas-Magana et al. 2014)	0.0003	0.0003
PTHALOS(600)	CMASS	Fitting Priors (Vargas-Magana et al. 2014)	0.0001	0.0004
PTHALOS(600)	CMASS	Fitting Nuisance T. (Vargas-Magana et al. 2014)	0.0005	0.0015
PTHALOS(600)	CMASS	Fitting Streaming (Vargas-Magana et al. 2014)	<0.0001	0.0005
PTHALOS(600)	CMASS	Fitting NL damping (Vargas-Magana et al. 2014)	0.0002	0.0009
Total 2			0.0007	0.0018
Total 1+Total 2			0.0023	0.0028

Table 21. Summary of Test Post-reconstruction: Best fitting values. We quote the maximal $\Delta\alpha$ and $\Delta\epsilon$ (eq.22) over the method variations not considered in the error budget of (Alam et al. 2016). We computed using the main table of the corresponding section (RMS of differences between the means obtained of each kind of variations and the fiducial case).

Mocks	Sample	Source of Uncertainty	$\Delta\alpha$	$\Delta\epsilon$
PATCHY(1000)	COMBINED	Estimator (all) (Section 4)	0.0012	0.0006
QPM(1000)	COMBINED	Randoms (Section 5)	0.0002	0.0002
PATCHY(1000)	COMBINED	Hexadecapole (Section 9)	0.0002	0.0002

Table 22. Distance constraints from the analysis of the BAO in the correlation functions of Combined Samples using the fiducial methodology. We quoted our results in the angle average distance $D_V(z)$, the Hubble parameter $H(z)$, the angular diameter $D_A(z)$, and the correlation $\rho_{D_A,H}$. We also quote α and ϵ with the statistical error. The sound horizon is evaluated using CAMB (Lewis et al. 2000). A fiducial $r_s^{\rm fid} = 147.78$ Mpc is assumed. The error bars in the constraints include the contribution from the systematic error budget. We quoted the two contributions to the error as $(x \pm \sigma_{\rm stat} \pm \sigma_{\rm sys})$ the total error is the sum in quadrature of both quantities $\sigma^2_{tot} = \sigma^2_{\rm stat} + \sigma^2_{\rm sys}$. For the systematic error we consider $\Delta\alpha = 0.002$, $\Delta\epsilon = 0.003$. The σ_{sys} considers $\rho_{\alpha,\epsilon} = 0$.

z	$D_V(z)r_s^{\rm fid}/r_s$ Mpc	$H(z)r_s/r_s^{\rm fid}$ km s^{-1} Mpc^{-1}	$D_A(z)r_s^{\rm fid}/r_s$ Mpc	$D_M = (1+z)D_A$ Mpc	$\rho_{D_A,H}$	α	ϵ
0.38	$1475 \pm 14 \pm 3$	$80.5 \pm 2.2 \pm 0.5$	$1092 \pm 16 \pm 4$	$1507 \pm 22 \pm 6$	0.47	0.9995 ± 0.0098	0.0152 ± 0.0125
0.51	$1872 \pm 16 \pm 4$	$90.9 \pm 2.1 \pm 0.6$	$1308 \pm 18 \pm 5$	$1975 \pm 27 \pm 8$	0.50	0.9928 ± 0.0084	-0.0036 ± 0.0107
0.61	$2131 \pm 20 \pm 4$	$99.1 \pm 2.5 \pm 0.6$	$1423 \pm 23 \pm 5$	$2291 \pm 37 \pm 8$	0.56	0.9820 ± 0.0091	-0.0109 ± 0.0125

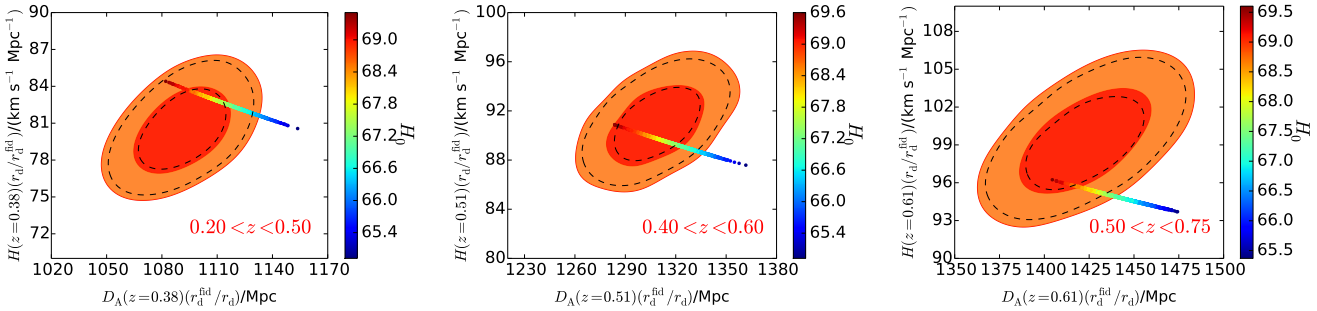

Figure 19. Constraints 1-2σ for $D_A(z)$ and $H(z)$ for the three samples at $z_{\rm eff} = 0.38, 0.51, 0.61$ from the fiducial methodology: multipoles analysis with MD-PATCHY covariance. Also included is the constraints from Planck 2015 temperature and polarisation power spectrum data assuming a ΛCDM model.

Ω_b, h. We found that the variations in the cosmology generate up to 0.0010 variations in the α, ϵ values.

• **Fitting/Modelling.** We explored a few sub percent uncertainties coming from the fitting methodology:

1) We tested the denominated "Modified Gaussian Damping Model" template against "Gaussian Damping Model" template used in a previous analysis. The observed variation in the mean are α is $\leqslant 0.0001$ and $\leqslant 0.0007$ in ϵ. The differences in the error distributions are 0.0003 in σ_α mean values, and $\leqslant 0.0020$ in σ_ϵ. The Modified Gaussian model gives smaller errors compared to the Gaussian model.

2) We tested the effects of considering the hexadecapole in the fits. The best fit results indicate that differences of using monopole+quadrupole compared with monopole+quadrupole+hexadecapole are not significant. The differences in α and ϵ are < 0.0002 post-reconstruction. The error distributions pre-reconstruction show a reduction of 0.0015 in all three redshift bins for σ_α and 0.0032 for σ_ϵ with respect to the fits monopole+quadrupole.

3) We revisited the fitting range and derived the optimal fitting range. We found an RMS variations of 0.0002 α and ϵ for different choices of the smallest/largest scale included in the fitting. We also found that by increasing upper bounds we can reduce the error about 0.0011 in α and 0.0019 in ϵ.

4) We revisited the dependence with the choice of bin centre. We found variations of 0.0002 on the mean values of α and 0.0004 on the mean values of ϵ. The error distributions are unchanged across the different bin centres. In σ_α and σ_ϵ, the dispersion is also approximately constant.

Based on this research we establish a systematic error budget for the new measurements. Our error budget do not consider correlations between variations of the methodology. i.e only considers changes in the methodology performed one-by-one. We find that $\sigma_\alpha^{sys} = 0.002$ and $\sigma_\epsilon^{sys} = 0.003$. We notice that the non-reconstruction related sources of theoretical systematic uncertainty in α all combine to make a contribution that is dominated by the uncertainty related to reconstruction techniques. The theoretical systematic uncertainty due to reconstruction is smaller for ϵ and is sub-leading compared to our upper bound of $\Delta\epsilon \approx 0.0025$, so that upper bound is essentially unchanged by reconstruction related systematics.

We have applied all the variations to the final DR12 Combined Sample of BOSS. The different measurements (except for the monopole+quadrupole+hexadecapole fits that lies in some cases outside bounds) in all three redshift are consistent with the mock catalogues results lying within $1-\sigma$ contours.

We have derived from the fiducial methodology fits the distance measurements for the three redshift bins of BOSS Combined Sample. The final constraints on the angular diameter distance $D_A(z)$ and the Hubble parameter $H(z)$, including statistical and theoretical systematic uncertainties, are 1.5% and 2.8% for the low redshift bin ($z_{\rm eff} = 0.38$), 1.4% And 2.4% for the intermediate redshift bin ($z_{\rm eff} = 0.51$), and 1.7% and 2.6% for the high redshift bin ($z_{\rm eff} = 0.61$). The constraints on $D_V(z)$ are 1.0%, 0.9% and 1.0% for the three redshift bins.

Finally our work serves also to evaluate alternative methodologies for future applications, i.e. to see if there would be demonstrable benefits from adopting any of the other approaches. Between the variations we explored in the paper we summarized the results of those that can be considered alternative choices to the usual clustering anisotropic BAO analysis:

• ω-estimator. Few BAO analyses have been performed using this clustering estimator, our results suggests this choice is preferred for BAO analysis as the errors are reduced.

• Model Covariance. We tested for the first time a model covariance approach from O'Connell et al. (2015) applied to an BOSS sample. We found that the performance of the model covariance is competitive with the sample covariance approach, validating its use in future surveys.

• Hexadecapole. We showed that the use of the hexadecapole decreases the mean error and the dispersion of the error distributions.

In the era of precision cosmology, the next generation dark energy experiments with galaxy surveys will push forward the precision of the measurements one order of magnitude, thus the comprehension of all sources of systematics errors will be critical for obtaining the sub percent precision required in the distance measurements. This contribution serves an starting point for future investigation in the theoretical systematics affecting the BAO-only distance measurements.

ACKNOWLEDGEMENTS

MV is partially supported by Programa de Apoyo a Proyectos de Investigación e Innovación Tecnológica (PAPITT) No IA102516 and Proyecto Conacyt Fronteras No 281. SH is supported by NSF AST1412966, NASA-EUCLID11-0004 and NSF AST1517593 for this work. AJC is supported by the European Research Coun-

cil under the European Community's Seventh Framework Programme FP7-IDEAS-Phys.LSS 240117. Funding for this work was partially provided by the Spanish MINECO under projects AYA2014-58747-P and MDM-2014-0369 of ICCUB (Unidad de Excelencia 'María de Maeztu'). G.R. is supported by the National Research Foundation of Korea (NRF) through NRF-SGER 2014055950 funded by the Korean Ministry of Education, Science and Technology (MoEST), and by the faculty research fund of Sejong University in 2016. AGS, JNG and SSA acknowledge support from the Trans-regional Collaborative Research Centre TR33 The Dark Universe of the German Research Foundation (DFG).

Funding for SDSS-III has been provided by the Alfred P. Sloan Foundation, the Participating Institutions, the National Science Foundation, and the U.S. Department of Energy Office of Science. The SDSS-III web site is http://www.sdss3.org/.

SDSS-III is managed by the Astrophysical Research Consortium for the Participating Institutions of the SDSS-III Collaboration including the University of Arizona, the Brazilian Participation Group, Brookhaven National Laboratory, University of Cambridge, Carnegie Mellon University, University of Florida, the French Participation Group, the German Participation Group, Harvard University, the Instituto de Astrofisica de Canarias, the Michigan State/Notre Dame/JINA Participation Group, Johns Hopkins University, Lawrence Berkeley National Laboratory, Max Planck Institute for Astrophysics, Max Planck Institute for Extraterrestrial Physics, New Mexico State University, New York University, Ohio State University, Pennsylvania State University, University of Portsmouth, Princeton University, the Spanish Participation Group, University of Tokyo, University of Utah, Vanderbilt University, University of Virginia, University of Washington, and Yale University.

This research used resources of the National Energy Research Scientific Computing Center, which is supported by the Office of Science of the U.S. Department of Energy under Contract No. DE-AC02-05CH11231.

REFERENCES

Planck Collaboration et al., 2015b, ArXiv e-prints, arXiv:1502.01589
Alam S. et al., 2015, ApJS, 219, 12
Alam S., et al., 2016, arXiv:1607.03155
Alcock C., Paczynski B., 1979, Nature, 281, 358.
Anderson L., et al., 2012, MNRAS, 427, 3435
Anderson L., et al., 2014, MNRAS, 439, 83
Anderson L., et al., 2014, MNRAS, 441, 24
Beutler F., et al., 2016, arXiv:1607.03149 (BAO)
Beutler F., et al., 2016, arXiv:1607.03150 (RSD)
Bolton A., et al., 2012, AJ, 144, 144
Bull P., Ferreira P. G., Patel P., Santos M. G., 2015, ApJ, 803, 21
Burden A., et al., 2014, MNRAS, 445, 3.
Burden A., Percival W. & Howlett C., 2015, MNRAS, 453, 456
Cuesta A. J., Vargas-Magaña M., Beutler F., et al., 2016, MNRAS, 457, 1770
Dawson K., et al., 2013, AJ, 145, 10
Dawson K. S., et al., 2016, AJ, 151, 44
Eisenstein D. J., Hu W., 1998, ApJ, 496, 605
Eisenstein D. J., Seo H.-J., Sirko E., Spergel D. N., 2007a, ApJ, 664, 675
Eisenstein D. J., Seo H.-J., White M., 2007b, ApJ, 664, 660
Eisenstein D. J., et al., 2011, AJ, 142.
Fisher K. B., Scharf C. A., Lahav O., 1994, MNRAS, 266, 219
Fukugita M., Ichikawa T., Gunn J. E., Doi M., Shimasaku K., Schneider D. P., 1996, AJ, 111, 1748
Gil-Marín H., Percival W. J., Cuesta A. J., et al., 2016, MNRAS, 460, 4210
Grieb M. et al. 2016, in prep (RSD wedges FS).
Gunn J. E., et al., 1998, AJ, 116, 3040.
Gunn J. E., et al., 2006, AJ, 131, 2332
Hartlap J., Simon P., & Schneider P. 2007, A&A, 464, 399
Kazin E., Sanchez A. G., Blanton M. R., 2012, MNRAS, 419, 3223
Kazin E., et al., 2013, MNRAS, 435, 64
Kitaura F.-S. et al., 2016, MNRAS, 456, 4156
Kitaura F.-S., Yepes G., Prada F., 2014, MNRAS, 439, L21
Klypin A., et al., 2016, MNRAS, 457, 4340
Landy S. D., Szalay A. S., 1993, ApJ, 412, 64
Laureijs R., 2009, ArXiv e-prints, arXiv:0912.0914
Laureijs R. et al., 2011, ArXiv e-prints, arXiv:1110.3193
Levi M. et al., 2013, ArXiv e-prints, arXiv:1308.0847
Lewis A., Challinor A., Lasenby A., 2000, ApJ, 538, 473
LSST Dark Energy Science Collaboration, 2012, ArXiv e-prints, arXiv:1211.0310.
Manera M., Scoccimarro R., Percival W. J., et al. 2013, MNRAS, 428, 1036
Matsubara T., Szalay, A. S. & Landy, S. D., The Astrophysical Journal, Volume 535, Issue 1, pp. L1-L4.
Mostek N. et al., 2012, in Society of Photo-Optical Instrumentation Engineers (SPIE) Conference Series, Vol. 8446, Society of Photo-Optical Instrumentation Engineers (SPIE) Conference Series, p. 0
Okumura T., et al., 2008, ApJ, 676, 889.
O'Connell R., Eisenstein D., Vargas M., Ho S., Padmanabhan N., 2015, arXiv:1510.01740
Padmanabhan N., et al., 2007, MNRAS, 378, 852
Padmanabhan N., White M., 2009, Phys. Rev. D, 80, 063508
Padmanabhan N., et al., 2012, MNRAS, 427, 2132
Paz D. J., Sánchez A. G., 2015, MNRAS, 454, 4326
Percival W. J., et al., MNRAS, 439, 2531.
Pope A. C.; Szapudi I., 2008, MNRAS, 389, 766
Reid B., et al., 2016, MNRAS, 455, 1553
Ross A. J., et al., 2011, MNRAS, 417, 1350
Ross A. J., Percival W. J., Sánchez A. G., et al., 2012, MNRAS, 424, 564.
Ross A. J., Percival W. J., & Manera M., 2015 MNRAS, 451, 1331
Ross A. J., et al., 2016, arXiv:1607.03145, MNRAS in press.
Satpathy S., et al., 2016, arXiv:1607.03148
Sánchez A. G., et al., 2013a, MNRAS, 433, 1201
Sánchez A. G., et al., 2016a, arXiv:1607.03147, MNRAS in press.
Sánchez A. G., et al., 2016b, arXiv:1607.03146, MNRAS in press.
Schneider M. D., Cole S., Frenk C. S., Szapudi I., 2011, ApJ, 737, 11
Scoccimarro R., Sheth R. K., 2002, MNRAS, 329, 629
Seo H.-J., Siegel E. R., Eisenstein D. J., White M., 2008, ApJ, 686, 13.
Seo H.-J., et al., 2010, ApJ, 720, 1650
Seo H.-J., et al., 2016, MNRAS, 460, 2453
Smee S., et al., 2013, AJ, 146, 32
Spergel D. et al., 2013a, ArXiv e-prints, arXiv:1305.5425
Spergel D. et al., 2013b, ArXiv e-prints, arXiv:1305.5422
de la Torre S., Peacock J. A., 2013, MNRAS, 435, 743
Vargas-Magana M., et al., 2014, MNRAS, 445, 2

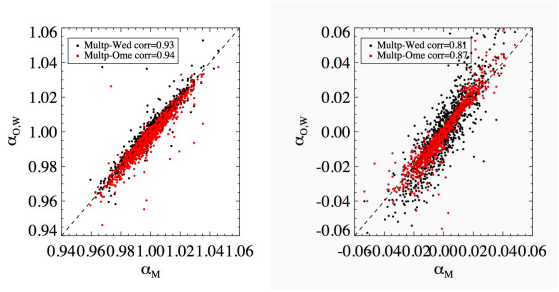

Figure A1. Dispersion plots of best fits from different clustering estimators $\xi_{0,2}, \xi_{\parallel,\perp}, \omega_l$ for 1000 MD-PATCHY post-reconstruction mocks for the lowest redshift bin. Left panel dispersion plots for α and right panel for ϵ. Similar plots are obtained for the intermediate and higher redshift bins.

Vargas-Magana M., Ho S., Cuesta A. J., Fromenteau S., 2015, ArXiv e-prints, arXiv:1509.06384.
White M., Tinker J. L., McBride C. K., 2014, MNRAS, 437, 2594
Xu X., et al., 2010, ApJ, 718, 1224.
Xu X., et al., 2012a, MNRAS, 427, 2146
Xu X., et al., 2012b, MNRAS, 431, 2834
Zhao C., et al., 2015, MNRAS 451, 4266

APPENDIX A: ESTIMATORS FITTING RESULTS

In Table C1 we show the results of performing the BAO anisotropic analysis to the 1000 MD-PATCHY mocks using different clustering estimators, pre and post-reconstruction. For the analysis in this section, we concentrate on the post-reconstruction results because those are the ones used for the BAO analysis; We focus first on the distributions of α and ϵ. The bias column of the table indicates the different estimators are unbiased estimators, $b_\alpha, b_\epsilon \leqslant 0.001$ for α and ϵ for multipoles and wedges, except for bin 2 where the bias in ϵ is slightly larger but still consistent with previous works ($b_\epsilon = 0.001 - 0.003$). In the case of ω-estimator, it shows a slightly larger bias in some bins compared to multipoles and wedges, its bias varies between 0.0004–0.003 in α and ϵ. Further investigation needs to be done to characterize the bias when using this estimator, we suspect varying the range should affect the results significantly, i.e there is still room to reduce the bias observed.

We now move on to discuss the dispersion of the distributions, the column of standard deviations indicates the distributions for α are very similar for all estimators($\Delta S_\alpha = 0.0001 - 0.0002$). However the ϵ distributions show larger scatter compared to the multipoles case, the differences in dispersion between ω and multipoles is $\Delta S_\epsilon^{\omega-M} = 0.0016 - 0.0025$, and between wedges and multipoles is $\Delta S_\epsilon^{\omega-M} = 0.0048 - 0.0057$.

As a crosscheck, we look at the consistency of the results. Figure A1 shows the scatter plots comparing the best fits obtained from using different estimators for the lower redshift bin (intermediate and higher bins show similar numbers and plots), on the left α and on the right ϵ. The correlation between best fit parameters using different estimators is high, the correlation between α coming from Multiples and those coming from ω analysis is $C_\alpha^{M-\omega} = 0.94$, the correlation between ϵ coming from Multiples and ϵ coming from wedges is $C_\alpha^{M-\omega} = 0.93$ and slightly lower for ϵ coming from Multiples and ϵ coming from ω, $C_\epsilon^{M-\omega} = 0.87$ and finally for ϵ coming from Multiples and ϵ coming from wedges is $C_\epsilon^{M-\omega} = 0.81$. The results indicate the consistency between the results obtained from the different estimators.

Table B1. Covariance Matrix Systematics. Fitting results from BOSS mocks pre-reconstruction.The different columns are the mean of the distributions of the best fits parameters and the respective uncertainties denoted by $\bar{x}$, the standard deviation of the distributions , denoted by S_x, the bias defined as the difference of the mean value compared to the expected value for the variable, $b_x = \bar{x} - x_{\rm exp}$, where $x_{\rm exp}$ is the expected value. There are few differences between the two analyses: the DR11 PTHALOS analysis was performed using a bin size of 8 h^{-1}Mpc compared to 5 h^{-1}Mpc used in the new QPM mocks; the fitting range has also changed, which improves the $\chi^2/d.o.f.$.

Covariance Matrix Systematics						
DR11 CMASS PATCHY-QPM NGC mocks, Pre-Reconstruction						
Cov	$\bar{\alpha}$	b_α	$\bar{\epsilon}$	b_ϵ	$\bar{\sigma_\alpha}$	$\bar{\sigma_\epsilon}$
PTHALOS	1.0044	0.0044	0.0021	0.0019	0.0153	0.0186
QPM	1.0027	0.0027	0.0011	0.0011	0.0191	0.0250

APPENDIX B: COMPARISON OF SAMPLE COVARIANCE MATRIX IN DR11: PTHALOS AND QPM.

We test the variations of BAO fitting results from the sample covariance in DR11 from two sets of mocks: PTHALOS (Manera et al. 2013a) used in previous data releases (DR9 , DR10, and DR11) and the new QPM mocks used in DR12 analysis. We limit this test to pre-reconstruction mock catalogues. The PTHALOS mocks are based on second order Lagrangian Perturbation Theory while the QPM mocks are generated from N-body simulations with big time steps. Although the QPM mocks have low resolution, they are expected to recover more of the non linearities to an order higher than the second; thus, we expect them to be more realistic than PTHALOS. These differences could impact the shifts observed in the pre-reconstruction results.

In Table B1 we show the fitting results obtained for the different sets of mocks; the results from PTHALOS were taken from Vargas-Magana et al. (2015). We start comparing the bias obtained from both mock catalogues, we find small differences in the bias values (~ 0.001). We find also small differences in the dispersion of the distributions of α and ϵ, $\Delta S_\alpha \sim 0.001$ and $\Delta S_\alpha \sim 0.002$.

The error distributions, when applying the methodology to both sets of mocks, are also in agreement. But QPM does result in larger error bars ($\Delta\sigma_\alpha = 0.0013$ and $\Delta\sigma_\epsilon = 0.0017$). The scatter differences are 0.0024 and 0.0042.

The fitting results are in reasonable agreement between both sets of mocks. The small differences we observe must be related to the differences on the methodology. The DR11 PTHALOS analysis was performed using a bin size of 8 h^{-1}Mpc compared to 5 h^{-1}Mpc used in the new QPM mocks; the fitting range has also changed, which improves the $\chi^2/d.o.f.$. However, it was shown in Vargas-Magana et al. (2014) that bin size has a < 0.001 bias effect from the best fitting parameters and 0.001 in the errors. We used the same values for the non-linear damping in both sets of mock catalogues: $(\Sigma_\parallel, \Sigma_\perp) = (6, 12)h^{-1}$ Mpc. It was also shown in Vargas-Magana et al. (2014), that variations in the non linear damping $\Sigma_{\parallel,\perp}$ affects the results in 0.001 or less in both best fitting values and the uncertainties. Because the cosmology of the mocks is slightly different, when we compare the covariances values, we are not able to disentangle the differences related to the mocks and the cosmology.

Table C1. Fitting results from MD-PATCHY mocks (pre) post-reconstruction (Section 4). The different columns are the mean of the distributions of the best fits parameters and their respective uncertainties denoted by $\bar{x}$, the standard deviation of the distributions, denoted by S_x, the bias defined as the difference of the mean value compared to the expected value for the variable, $b_x = \bar{x} - x_{\rm exp}$, where $x_{\rm exp}$ is the expected value.

2-Point Statistics Estimator Systematics						
DR12 Combined MD-PATCHY mocks, Pre-Reconstruction						
Est	$\bar{\alpha}$	b_α	$\bar{\epsilon}$	b_ϵ	$\bar{\sigma}_\alpha$	$\bar{\sigma}_\epsilon$
Bin 1 ($0.2 < z < 0.5$)						
ξ_ℓ	1.0015	0.0022	−0.0003	−0.0005	0.0262	0.0334
$\xi_{\parallel,\perp}$	1.0084	0.0091	0.0081	0.0079	0.0276	0.0412
ω_ℓ	0.9973	−0.0020	−0.0042	−0.0044	0.0206	0.0273
Bin 2 ($0.4 < z < 0.6$)						
ξ_ℓ	1.0038	0.0042	0.0014	0.0012	0.0222	0.0291
$\xi_{\parallel,\perp}$	1.0080	0.0084	0.0067	0.0065	0.0237	0.0375
ω_ℓ	0.9993	−0.0003	−0.0027	−0.0030	0.0219	0.0287
Bin 3 ($0.5 < z < 0.75$)						
ξ_ℓ	1.0039	0.0040	0.0003	0.0001	0.0215	0.0282
$\xi_{\parallel,\perp}$	1.0071	0.0072	0.0079	0.0077	0.0221	0.0363
ω_ℓ	0.9996	−0.0003	−0.0027	−0.0031	0.0176	0.0244
DR12 Combined MD-PATCHY mocks, Post-Reconstruction						
Est	$\bar{\alpha}$	b_α	$\bar{\epsilon}$	b_ϵ	$\bar{\sigma_\alpha}$	$\bar{\sigma_\epsilon}$
Bin 1 ($0.2 < z < 0.5$)						
ξ_ℓ	0.9986	−0.0007	0.0009	0.0007	0.0147	0.0188
$\xi_{\parallel,\perp}$	0.9988	−0.0005	0.0006	0.0004	0.0145	0.0217
ω_ℓ	0.9967	−0.0026	0.0012	0.0010	0.0122	0.0168
Bin 2 ($0.4 < z < 0.6$)						
ξ_ℓ	1.0006	0.0010	0.0023	0.0021	0.0130	0.0163
$\xi_{\parallel,\perp}$	1.0009	0.0013	0.0033	0.0031	0.0129	0.0197
ω_ℓ	0.9992	−0.0004	0.0030	0.0027	0.0130	0.0196
Bin 3 ($0.5 < z < 0.75$)						
ξ_ℓ	1.0007	0.0008	0.0011	0.0009	0.0133	0.0166
$\xi_{\parallel,\perp}$	1.0009	0.0010	0.0017	0.0015	0.0130	0.0203
ω_ℓ	0.9989	−0.0010	0.0011	0.0007	0.0112	0.0152

Table C2. Covariance Matrix Systematics. Fitting results from BOSS mocks post-reconstruction. The different columns are the mean of the distributions of the best fits parameters and the respective uncertainties denoted by $\bar{x}$, the standard deviation of the distributions , denoted by S_x, the bias defined as the difference of the mean value compared to the expected value for the variable, $b_x = \bar{x} - x_{\rm exp}$, where $x_{\rm exp}$ is the expected value.

Covariance Matrix Systematics: Sample Covariance from Different simulations.						
DR12 Combined Sample PATCHY mocks, Pre-Reconstruction						
S-C	$\bar{\alpha}$	b_α	$\bar{\epsilon}$	b_ϵ	$\bar{\sigma_\alpha}$	$\bar{\sigma_\epsilon}$
BIN 1 ($0.2 < z < 0.5$)						
P-P	1.0015	0.0022	−0.0003	−0.0005	0.0262	0.0334
Q-Q	0.9801	0.0034	0.0028	0.0026	0.0224	0.0320
BIN 2 ($0.4 < z < 0.6$)						
P-P	1.0038	0.0042	0.0014	0.0012	0.0222	0.0291
Q-Q	0.9838	0.0046	0.0035	0.0033	0.0198	0.0280
BIN 3 ($0.5 < z < 0.75$)						
P-P	1.0039	0.0040	0.0003	0.0001	0.0215	0.0282
Q-Q	0.9842	0.0032	0.0038	0.0036	0.0198	0.0280
DR12 Combined Sample PATCHY/QPM mocks, Post-Reconstruction						
BIN 1 ($0.2 < z < 0.5$)						
P-P	0.9986	−0.0007	0.0009	0.0007	0.0147	0.0188
P-P*	0.9989	−0.0004	0.0011	0.0009	0.0188	0.0253
P-Q	0.9989	−0.0004	0.0007	0.0005	0.0138	0.0174
Q-Q	0.9797	0.0030	0.0032	0.0030	0.0136	0.0190
Q-P	0.9802	0.0035	0.0028	0.0026	0.0144	0.0209
BIN 2 ($0.4 < z < 0.6$)						
P-P	1.0006	0.0010	0.0023	0.0021	0.0130	0.0163
P-P*	1.0003	0.0007	0.0025	0.0023	0.0153	0.0207
P-Q	0.9989	−0.0007	0.0010	0.0008	0.0128	0.0156
Q-Q	0.9805	0.0013	0.0043	0.0041	0.0125	0.0172
Q-P	0.9818	0.0026	0.0049	0.0047	0.0124	0.0177
BIN 3 ($0.5 < z < 0.75$)						
P-P	1.0007	0.0008	0.0011	0.0009	0.0133	0.0166
P-P*	1.0004	0.0005	0.0001	−0.0001	0.0156	0.0204
P-Q	1.0005	0.0006	−0.0000	−0.0002	0.0137	0.0163
Q-Q	0.9822	0.0012	0.0046	0.0044	0.0130	0.0179
Q-P	0.9817	0.0007	0.0059	0.0057	0.0128	0.0181

APPENDIX C: TABLES

APPENDIX D: CORRELATION MATRICES

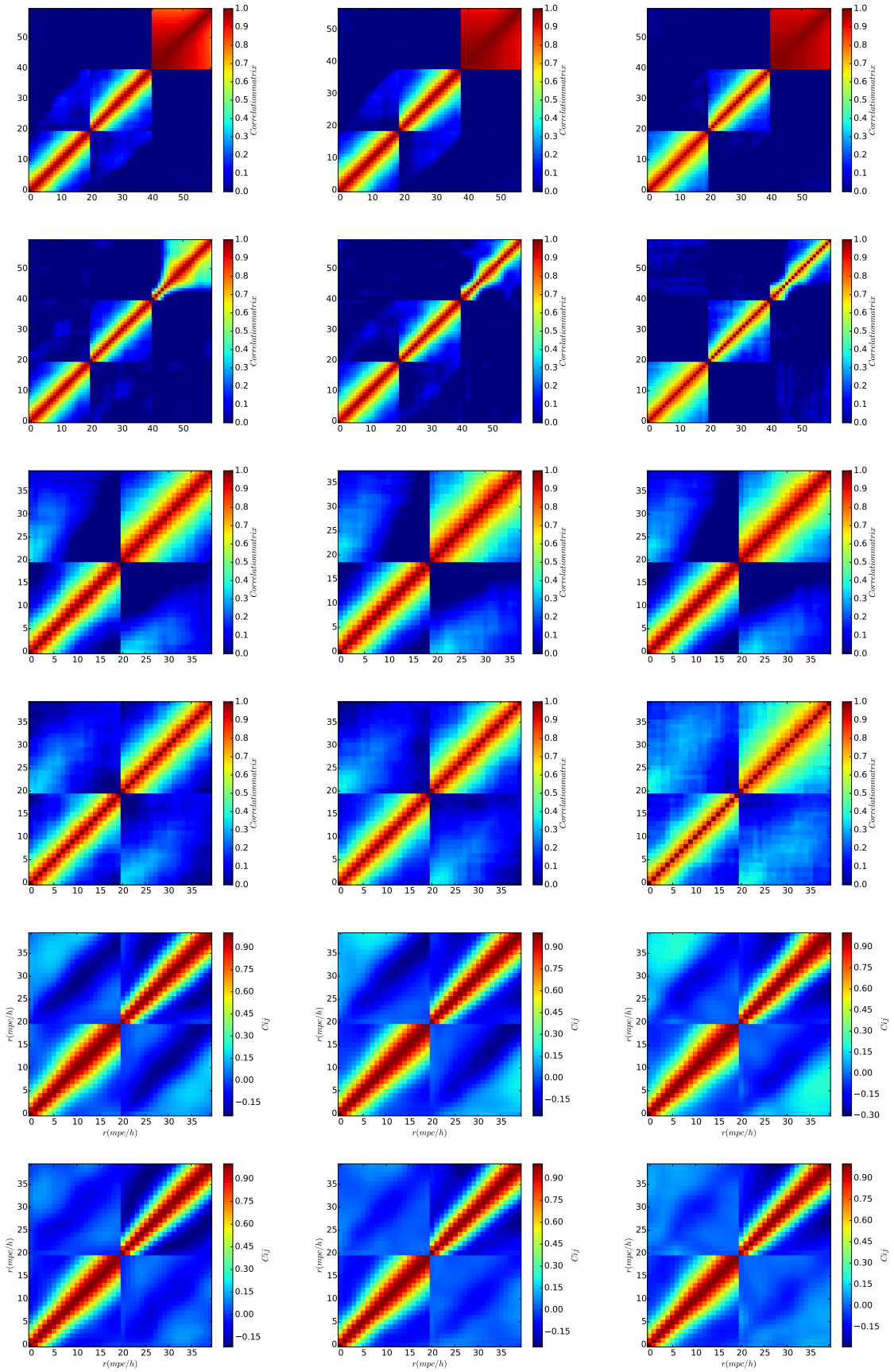

Figure D1. Correlation matrix pre-reconstruction (top) and post-reconstruction (bottom) for MD-PATCHY for 1000 for the 3 redshift bins.Top panels: Multipoles Clustering Estimator including Hexadecapole. Intermediate panels: Wedges clustering estimator. Bottom panels. $\omega-$Clustering Estimator.

Table C3. Covariance Matrix Systematics. Fitting results from BOSS mocks post-reconstruction.The different columns are the mean of the distributions of the best fits parameters and the respective uncertainties denoted by $\bar{x}$, the standard deviation of the distributions , denoted by S_x, the bias defined as the difference of the mean value compared to the expected value for the variable, $b_x = \bar{x} - x_{\rm exp}$, where $x_{\rm exp}$ is the expected value.

Covariance Matrix Systematics: Model Covariance.						
DR12 Combined Sample PATCHY mocks, Pre-Reconstruction						
Cov	$\bar{\alpha}$	b_α	$\bar{\epsilon}$	b_ϵ	$\bar{\sigma_\alpha}$	$\bar{\sigma_\epsilon}$
Bin 1 ($0.20 < z < 0.50$)						
M	1.0011	0.0018	−0.0007	−0.0009	0.0260	0.0343
S	1.0015	0.0022	−0.0003	−0.0005	0.0262	0.0334
Bin 2 ($0.40 < z < 0.60$)						
M	1.0035	0.0039	0.0009	0.0007	0.0225	0.0293
S	1.0038	0.0042	0.0014	0.0012	0.0222	0.0291
Bin 3 ($0.50 < z < 0.75$)						
M	1.0038	0.0039	0.0001	−0.0001	0.0219	0.0287
S	1.0039	0.0040	0.0003	0.0001	0.0215	0.0282
DR12 Model Covariance, Post-Reconstruction						
Bin 1 ($0.20 < z < 0.50$)						
M	0.9988	−0.0005	0.0009	0.0007	0.0144	0.0190
S	0.9986	−0.0007	0.0009	0.0007	0.0147	0.0188
Bin 2 ($0.40 < z < 0.60$)						
M	1.0001	0.0005	0.0016	0.0014	0.0130	0.0171
S	1.0006	0.0010	0.0023	0.0021	0.0130	0.0163
Bin 3 ($0.50 < z < 0.75$)						
M	1.0004	0.0005	0.0003	0.0001	0.0133	0.0166
S	1.0007	0.0008	0.0011	0.0009	0.0133	0.0166

Table C4. Random catalogue test. Results of the BAO anisotropic fitting of QPM mocks Post-Reconstruction when the size of the random catalogue is varied. The different columns are the mean of the distributions of the best fits parameters denoted by $\bar{x}$, the standard deviation of the distributions , denoted by S_x, the bias defined as the difference of the mean value compared to the expected value for the variable, $b_x = \bar{x} - x_{\rm exp}$, where $x_{\rm exp}$. Since the fiducial cosmology is not the natural cosmology of QPM mocks, the expected values for α and ϵ are: $\alpha_{\rm exp}$ = (0.9767,0.9792,0.9810), $1 + \epsilon_{\rm exp}$=(1.0017,1.0023,1.0027). We use the covariance from 1000 QPM mocks . The case label as 4x means 4x for SS pair-counts and 50x for SR pair-counts.

Correlation Function Systematics: Random Systematics						
DR12 Combined Sample QPM mocks, Post-Reconstruction						
Imp	$\bar{\alpha}$	S_α	b_α	$\bar{\epsilon}$	S_ϵ	b_ϵ
Bin 1 50x	0.9782	0.0120	0.0015	0.0033	0.0174	0.0016
Bin 2 50x	0.9804	0.0107	0.0012	0.0038	0.0134	0.0015
Bin 3 50x	0.9826	0.0110	0.0016	0.0051	0.0131	0.0024
Bin 1 4x	0.9780	0.0122	0.0013	0.0031	0.0183	0.0014
Bin 2 4x	0.9803	0.0110	0.0011	0.0038	0.0134	0.0015
Bin 3 4x	0.9827	0.0112	0.0017	0.0051	0.0130	0.0024

Table C5. Fiducial cosmology related systematics. Fitting results from QPM NGC mocks pre-/post- reconstruction using a different cosmology in the analysis from the natural cosmology of the mocks. Anderson and Cosmology 3 are flat cosmologies that are shifted in Ω_m by 0.5% compared to QPM cosmology, but exactly the same Ω_b, h. The different columns are the mean of the distributions of the best fits parameters denoted by $\bar{x}$, the standard deviation of the distributions , denoted by S_x, the bias defined as the difference of the mean value compared to the expected value for the variable, $b_x = \bar{x} - x_{\rm exp}$, where $x_{\rm exp}$ is the expected value. The expected shifts are: $\alpha_{\rm exp}^{\rm QPM} = 1.0$, $\epsilon_{\rm exp}^{\rm QPM} = 0.0$,$\alpha_{\rm exp}^{\rm And} = 1.0064$, $\epsilon_{\rm exp}^{\rm And} = -0.0021$ Test post-reconstruction where performed with N_{sim} =96 mocks, $\sqrt{N_{sim}} \sim 9.8$

Fiducial Cosmology related Systematics						
DR11 CMASS QPM mocks, Pre-Reconstruction						
Cosmo	$\bar{\alpha}$	S_α	b_α	$\bar{\epsilon}$	S_ϵ	b_ϵ
AND	1.0083	0.0215	0.0019	-0.0021	0.0313	<0.0001
QPM	1.0024	0.0213	0.0024	-0.0001	0.0303	0.0001
DR11 CMASS QPM mocks, Post-Reconstruction						
AND	1.0061	0.0152	-0.0003	-0.0014	0.0197	0.0005
QPM	0.9994	0.0153	0.0006	0.0015	0.0206	0.0015

Table C6. Reconstruction related systematics. Fitting results from Patchy NGC mocks Post-reconstruction using different smoothing scale in the reconstruction of the density field. The different columns are the mean of the distributions of the best fits parameters denoted by $\bar{x}$, the standard deviation of the distributions , denoted by S_x, the bias defined as the difference of the mean value compared to the expected value for the variable, $b_x = \bar{x} - x_{\rm exp}$, where $x_{\rm exp}$. The expected shifts are: $\alpha_{exp}^{\rm PATCHY} = 0.9993$, $\epsilon_{exp}^{\rm PATCHY} = 0.0002$

Reconstruction related Systematics						
DR12 PATCHY Combined mocks Bin 2, Post-Reconstruction						
Smoothing	$\bar{\alpha}$	S_α	b_α	$\bar{\epsilon}$	S_ϵ	b_ϵ
5	0.9995	0.0137	0.0002	-0.0011	0.0096	-0.0013
10	1.0026	0.0138	0.0033	-0.0004	0.0125	-0.0006
15	1.0016	0.0139	0.0024	-0.0002	0.0129	-0.0004

Table C7. Fitting Related Systematics. Fitting results from PATCHY DR12 Combined Sample mocks post-reconstruction. The different columns are the mean of the distributions of the best fits parameters and the respective uncertainties denoted by $\bar{x}$, the standard deviation of the distributions , denoted by S_x, the bias defined as the difference of the mean value compared to the expected value for the variable, $b_x = \bar{x} - x_{\rm exp}$, where $x_{\rm exp}$ is the expected value.

Fitting Methodology Systematics						
DR12 Combined Sample PATCHY mocks, Post-Reconstruction						
$C_{G,MG}$	$\bar{\alpha}$	b_α	$\bar{\epsilon}$	b_ϵ	$\bar{\sigma_\alpha}$	$\bar{\sigma_\epsilon}$
Bin 3 ($0.2 < z < 0.5$)						
C_G	0.9986	-0.0007	0.0009	0.0007	0.0147	0.0188
C_{MG}	0.9986	-0.0007	0.0013	0.0011	0.0150	0.0207
Bin 3 ($0.4 < z < 0.6$)						
C_G	1.0006	0.0010	0.0023	0.0021	0.0130	0.0163
C_{MG}	1.0006	0.0010	0.0025	0.0023	0.0137	0.0185
Bin 3 ($0.5 < z < 0.75$)						
C_G	1.0007	0.0008	0.0011	0.0009	0.0133	0.0166
C_{MG}	1.0006	0.0007	0.0010	0.0008	0.0137	0.0185

Table C8. Fitting Related Systematics. Fitting results from PATCHY DR12 Combined Sample mocks pre/post-reconstruction. The different columns are the mean of the distributions of the best fits parameters and the respective uncertainties denoted by $\bar{x}$, the standard deviation of the distributions , denoted by S_x, the bias defined as the difference of the mean value compared to the expected value for the variable, $b_x = \bar{x} - x_{\rm exp}$, where $x_{\rm exp}$ is the expected value.

Fitting Methodology Systematics: hexadecapole contribution						
DR12 Combined Sample PATCHY, Pre-Reconstruction						
Multp	$\bar{\alpha}$	b_α	$\bar{\epsilon}$	b_ϵ	$\bar{\sigma_\alpha}$	$\bar{\sigma_\epsilon}$
Bin 1 ($0.2 < z < 0.5$)						
$\xi_{l=2}$	1.0015	0.0022	-0.0003	-0.0005	0.0262	0.0334
$\xi_{l=4}$	1.0017	0.0024	0.0001	-0.0001	0.0204	0.0242
Bin 2 ($0.4 < z < 0.6$)						
$\xi_{l=2}$	1.0038	0.0042	0.0014	0.0012	0.0222	0.0291
$\xi_{l=4}$	1.0036	0.0040	0.0011	0.0009	0.0196	0.0227
Bin 3 ($0.5 < z < 0.75$)						
$\xi_{l=2}$	1.0039	0.0040	0.0003	0.0001	0.0215	0.0282
$\xi_{l=4}$	1.0039	0.0040	0.0003	0.0001	0.0112	0.0137
DR12 Combined Sample PATCHY, Post-Reconstruction						
Bin 1 ($0.2 < z < 0.5$)						
$\xi_{l=2}$	0.9986	-0.0007	0.0009	0.0007	0.0147	0.0188
$\xi_{l=4}$	0.9984	-0.0009	0.0006	0.0004	0.0154	
Bin 2 ($0.4 < z < 0.6$)						
$\xi_{l=2}$	1.0006	0.0010	0.0023	0.0021	0.0130	0.0163
$\xi_{l=4}$	1.0003	0.0007	0.0020	0.0018	0.0116	0.0133
Bin 3 ($0.5 < z < 0.75$)						
$\xi_{l=2}$	1.0007	0.0008	0.0011	0.0009	0.0133	0.0166
$\xi_{l=4}$	1.0007	0.0008	0.0011	0.0009	0.0119	0.0136

Table C9. Fitting Related Systematics: Fitting results from PATCHY DR12 Combined Sample mocks post-reconstruction for the intermediate redshift bin. The different columns are the mean of the distributions of the best fits parameters and the respective uncertainties denoted by $\bar{x}$, the standard deviation of the distributions , denoted by S_x, the bias defined as the difference of the mean value compared to the expected value for the variable, $b_x = \bar{x} - x_{\rm exp}$, where $x_{\rm exp}$ is the expected value.

Fitting Methodology Systematics: Range						
DR12 Combined Sample Bin 2 PATCHY mocks, Post-Reconstruction						
R_{min}	$\bar{\alpha}$	b_α	$\bar{\epsilon}$	b_ϵ	$\bar{\sigma_\alpha}$	$\bar{\sigma_\epsilon}$
30	1.0037	0.0041	0.0036	0.0034	0.0112	0.0137
40	1.0007	0.0011	0.0025	0.0023	0.0127	0.0158
50	1.0007	0.0011	0.0025	0.0023	0.0128	0.0157
60	1.0006	0.0010	0.0023	0.0021	0.0130	0.0163
70	0.9989	−0.0007	0.0012	0.0010	0.0126	0.0143
80	1.0201	0.0208	0.0252	0.0248	0.0191	0.0337
DR12 Combined Sample Bin 2 PATCHY mocks, Post-Reconstruction						
120	1.0013	0.0017	0.0012	0.0010	0.0163	0.0216
130	0.9995	−0.0001	0.0013	0.0011	0.0153	0.0202
140	1.0001	0.0005	0.0019	0.0017	0.0142	0.0185
155	1.0006	0.0010	0.0023	0.0021	0.0130	0.0163
160	1.0005	0.0009	0.0021	0.0019	0.0129	0.0161
170	1.0007	0.0011	0.0022	0.0020	0.0119	0.0144
180	1.0007	0.0011	0.0023	0.0021	0.0118	0.0142

Table C10. Fitting Related Systematics. Fitting results from PATCHY DR12 Combined Sample mocks post-reconstruction for the intermediate redshift bin. The different columns are the mean of the distributions of the best fits parameters and the respective uncertainties denoted by $\bar{x}$, the standard deviation of the distributions , denoted by S_x, the bias defined as the difference of the mean value compared to the expected value for the variable, $b_x = \bar{x} - x_{\rm exp}$, where $x_{\rm exp}$ is the expected value.

Fitting Methodology Systematics: Bin Centre						
DR12 Combined Sample Bin 2 PATCHY mocks, Post-Reconstruction						
Centre	$\bar{\alpha}$	S_α	b_α	$\bar{\epsilon}$	S_ϵ	b_ϵ
0 h^{-1}Mpc	1.0006	0.0118	0.0010	0.0023	0.0132	0.0021
1 h^{-1}Mpc	1.0004	0.0118	0.0008	0.0023	0.0132	0.0021
2 h^{-1}Mpc	1.0006	0.0117	0.0010	0.0019	0.0130	0.0017
3 h^{-1}Mpc	1.0003	0.0121	0.0007	0.0017	0.0138	0.0015
4 h^{-1}Mpc	1.0005	0.0118	0.0009	0.0020	0.0134	0.0018